1 2 3	Short title: Removal of Cation/H ⁺ Exchangers (CAXs)	
4 5 6	Removal of Cation/H ⁺ Exchangers (CAXs) Reveals their Additive Role in H ⁺ /Ca ²⁺ exchange, Calcium Accumulation, Signaling and Elemental Repartitioning	
7	Iny Elizebeth Mathew ¹ , Hormat Shadgou Rhein ¹ , Jian Yang ¹ , Armando Carpaneto ^{2,3} , Antonella	
8	Gradogna², Qi Guo⁴, Ryan Tappero⁵, Joachim Scholz-Starke², Bronwyn J. Barkla⁴, Kendal D.	
9	Hirschi ^{1&} , and Tracy Punshon ⁶	
10		
11	¹ Pediatrics-Nutrition, Children's Nutrition Research, Baylor College of Medicine, Houston, TX,	
12	77030, USA	
13	² Institute of Biophysics, Consiglio Nazionale delle Ricerche, Via de Marini 6, 16149 Genova, Italy	
14	³ Department of Earth, Environment and Life Sciences (DISTAV), University of Genoa, Viale	
15	Benedetto XV 5, 16132 Genova, Italy	
16 17 18 19	³ Center for Research in Agricultural Genomics, Consejo Superior de Investigaciones Científicas, Barcelona, Spain	
	⁴ Faculty of Science and Engineering, Southern Cross University	
20	Lismore, New South Wales, Australia	
21 22 23 24	⁵Photon Sciences Department, Brookhaven National Laboratory, Upton, NY 11973	
	⁶ Department of Biological Sciences, Dartmouth College, Hanover, NH, 03755 USA	
25		
26		
27		
28	^{&} Corresponding Author: Kendal Hirschi	
29	Email: kendalh@bcm.edu	

30	The author responsible for the distribution of materials integral to the findings presented in this		
31	article in accordance with the policy described in the Instructions for Authors		
32	(https://academic.oup.com/pphys/pages/General-Instructions) is Kendal Hirschi		
33	Keywords		
34	Calcium, Transport, Signaling, SXRF, Vacuole		
35 36 37	One-sentence summary. Removal of Cation/H ⁺ Exchangers (CAXs) have pleiotropic effects on signaling, elemental distribution, and stress responses.		
38	Author Contributions		
39 40 41 42	R.T. and K.D.H performed research, T.P, J.Y, I.E.M, R.B., H.S.R, Q.G., B.B., J.S.S. and K.D.H analyzed data. T.P., I.E.M, H.S.R., Q.G., B.B., J.S.S. and K.D.H wrote paper.		
43			
44	Word Count:		
45	Figures: 8		
46	Running title: Anoxia Tolerance and H ⁺ /Cation Transport		
47			
48			

Abstra	act
--------	-----

50

51

52

53

54

55

56

57

58

59

60

61

62

63

64

65

Four Arabidopsis H⁺/Cation exchangers (CAXs) participate in high-capacity cation transport into the vacuole. The impaired function of CAX1 (cax1) provokes both stress sensitivities and anoxia tolerance; however, other CAXs make assessing loss of H⁺/Cation transport enigmatic. Here, we generated an Arabidopsis thaliana mutant defective in four CAXs. These quadruple mutants (cax1-4: gKO) exhibited reduced growth, diminished fertility, and an 85% reduction in tonoplast localized H⁺/Ca transport. Elemental imaging using SXRF in combination with ICP-MS showed changes in metal partitioning and reduced calcium (Ca) abundance in qKO leaf tissue. In contrast to the impaired growth of qKO in normoxia conditions (ambient oxygen levels), anoxia tolerance was improved more than in cax1. The anoxia tolerance appeared to be caused by reduced endogenous calcium levels; wild-type plants grown in reduced calcium conditions were anoxia tolerant. Sequential reduction of CAXs increased mRNA expression changes and proteins associated with Reactive Oxygen Species, Ca, and stress signaling pathways. Using a genetically encoded Ca indicator (GECI), mutations in multiple CAXs heightened changes in post-anoxia Ca signaling. The quadruple CAX mutant provides a resource to uncover the role of diminished tonoplast localized H⁺/Ca transport and altered elemental repartitioning in plant signaling and stress responses.

66

67

68 69

Introduction

Control of calcium (Ca) ion concentrations is critical for plant function; it is a cell wall component, an enzyme cofactor and a second messenger (26). Calcium homeostasis is dependent on transporters, including ion-coupled transporters like the Na⁺/Ca²⁺ exchanger (NCX), Na⁺/Ca²⁺, K⁺ exchanger (NCKX), cation/Ca²⁺ exchanger (CCX) and H⁺/Cation exchanger (CAX), which are members of the CaCA superfamily (8; 41). Calcium pumps and exchangers are located in multiple membrane systems, including the endoplasmic reticulum (ER), tonoplast, and plasma membrane (PM) (18). Calcium pumps are considered low-capacity, high-affinity efflux systems, but within this broad group of transporters, CAXs are distinct because they have high capacity and low affinity (40). While both Ca pumps and CAXs remove Ca from the cytoplasm, their contributions to controlling the magnitude or duration of different stimulus-specific Ca signals remains enigmatic.

Calcium can accumulate to millimolar levels in the vacuole, but levels are maintained in the range of nanomolar to low micromolar in the cytosol (35; 47). This steep concentration gradient is established with the help of high-capacity H⁺/Ca exchange and Ca pumping (51). The driving force for cation antiport activity is the pH gradient generated by two electrogenic proton pumps located on the membrane, an ATPase and a pyrophosphatase (PPase) (50). H⁺ transport processes are integrated with many transport functions (48), such as trafficking and hormone perception (20; 49); these processes involve alterations in Ca levels, and H⁺/Ca exchangers may play an importantessential role in Ca and pH related signaling events (42).

Plant H⁺/Cation exchangers were cloned using a yeast complementation approach (27). A limitation of many previous CAX studies has been the reliance on yeast assays as a proxy for plant-based studies (40). Both yeast and plant studies suggest that CAXs function in the transport of Ca and numerous other cations (40). CAX transporters are found in multiple species (40), suggesting a pivotal role. There are six CAXs in Arabidopsis Arabidopsis has six CAXs, but only CAX1-4 are expressed (33). CAX2 and CAX4 are expressed at lower levels in plants, and

most of the work on CAXs in plants has focused on the more highly expressed CAX1 and CAX3 (16).CAX1 is expressed in aerial tissues, and CAX3 is primarily expressed primarily in the roots (28). Expression of CAX3 is increased in leaves/shoots during stresses such as wounding. There is some evidence that CAX1 and CAX3 may function as heterodimers (28), because they are coexpressed in guard cells where they may function singly or together in intracellular signaling (30). During stress responses (pathogen attack, temperature fluctuations), absence of CAX1 induces ectopic expression of other CAXs, which may help maintain some cellular secretion of Ca to the apoplast (12). High-resolution elemental imaging via synchrotron X-ray fluorescence (SXRF) has shown that cax1 alters Ca partitioning within cells, reducing Ca partitioning into organelles and/or increasing Ca in the cytosol and abolishing tissue-level Ca gradients (43). cax1 also has subtle phenotypes in standard growth conditions (11) but increased tolerance to anoxia (53), serpentine soils (6), freezing (10) as well as altered metal sensitivity (3), and pathogen defense responses (53). Meanwhile, mutations in both CAX1 and CAX3 cause a significant reduction in plant stature and fertility while maintaining 50% of the tonoplast H+/Ca exchange. There is interplay between CAXs and other transporters; deletions in CAX1 reduce the activities of tonoplast Ca(2+)/H(+) antiporter, tonoplast V-type H(+)-ATPase and increase the activities of tonoplast Ca(2+)-ATPase and vacuolar Ca(2+)/H(+) antiporters like CAX3 and CAX4 (11). Given this regulatory (12)growth and development. Utilizing a battery of phenotyping, omics, and imaging techniques, we investigate how the loss of four CAXs impacts growth, membrane transport, elemental distribution, and signaling. These findings establish the ability to significantly reduce tonoplast H⁺/Ca exchange and the utility of reducing leaf calcium content by sequentially removing CAXs.

Results

122

121

97

98

99

100

101

102

103

104

105

106

107

108

109

110

111

112

113

114

115

116

117

118

119

123 Growth characteristics of Arabidopsis lines lacking multiple Ca/H⁺ antiporters CAX1 has been known to regulate intracellular Ca²⁺ levels. Plants deficient in CAX1 exhibit 124 Mn²⁺ and Mg²⁺ stress tolerance, a slightly altered ionome and perturbed hormone sensitivities 125 126 (11; 12). Further, cax1 is anoxia and submergence tolerant (53), although none of the other 127 three single CAX mutants showed this phenotype (53). To determine if impairing these other 128 CAXs had an additive effect on various phenotypes exhibited by cax1, we generated lines 129 lacking multiple CAX transporters. 130 Plants without both CAX1 and CAX3 (dKO-cax1/3) have been previously generated (12) 131 while triple (tKO-cax1/cax3/cax4) and quadruple mutants (qKO-cax1/cax2/cax3/cax4) were 132 developed in this study. These mutants, like dKO, displayed alterations in growth and 133 development as plants matured (Figure 1), although there were no significant differences in their 134 germination. During the first several weeks of growth on normal media, these mutants displayed 135 little growth difference compared to Col-0 and cax1. However, transferring the seedlings to 136 media supplemented with 25 mM CaCl₂ reduced their growth (Figure 1A). A similar result was 137 obtained when the plants were grown in hydroponic basal nutrient solution (BNS) containing 1 138 mM Ca (Figure 1B) (16); dKO, tKO, and qKO lines grew less than Col-0 and cax1 (Figure 1B). 139 However, when grown hydroponically in a low Ca solution (LCS), this growth difference was 140 reversed, the dKO, tKO, and qKO lines had enhanced growth compared to Col-0 (LCS, 141 0.025mM Ca; Supplemental Figure 1). 142 Various developmental defects were also observed when plants were grown on half-MS media 143 (10 days old) and transferred to soil. Again, dKO, tKO, and qKO lines grew less and slower than 144 Col-0 and the CAX single mutants. As reported previously for dKO (12), tKO and the gKO plants 145 were bushy due to continued lateral branching and nectrotic leaf tips (Figure 1C; Supplemental 146 Figure 2A). Further, dKO, tKO, and gKO did not produced appreciable amounts of viable 147 siliques/seeds (Supplemental Figure 2B). The siliques that did form were small and twisted.

However, the dKO, tKO, and qKO lines grew well and produced viable seeds when germinated and grown to maturity in LCS.

Transport Measurements

To evaluate the vacuolar Ca uptake capacity of the qKO mutant, we performed combined patch-clamp and microfluometry experiments (9; 23) on isolated Arabidopsis mesophyll vacuoles, in which the ratiometric Ca indicator dye fura-2 (24) was loaded into the vacuolar lumen through the patch pipette. After equilibration with the pipette solution, vacuoles were exposed to bath solutions containing high Ca concentrations and the resulting changes in vacuolar fura-2 fluorescence were monitored (Supplemental Figure 3). In Col-0 vacuoles, bath application of 10 μ M or 30 μ M Ca evoked fast and robust increases of the vacuolar Ca concentration, which were fully reversible upon washout (Figure 2A, C). qKO vacuoles showed diminished vacuolar [Ca²⁺] increases at 10 μ M Ca (94% reduction compared to Col-0) and attenuated responses at 30 μ M Ca in the bath solution (85% reduction compared to Col-0) (Figure 2B, C). These data suggest that, under our experimental conditions, CAX proteins are responsible for Ca uptake capacity in Arabidopsis vacuoles.

Elemental Analysis

The role of CAX transporters in partitioning elements within the leaf has yet to be investigated. Elemental imaging of the qKO lines allowed us to see how loss of four CAXs impacts mineral distribution and abundance in leaves under normal growth conditions. We collected elemental data using two contrasting techniques. Volume-averaged (bulk) concentration data (N=3) was collected from dried, digested tissue from multiple plants via inductively coupled plasma mass spectrometry (ICP-MS), and spatially resolved abundances were imaged in fresh, size-matched Col-0 and mutant leaves in the same map (N=3) using synchrotron X-ray fluorescence (SXRF)

mapping. Our previous elemental imaging analysis (43) on vacuolar Ca partitioning was conducted on chemically fixed, embedded, and sectioned embryonic tissue.

Bulk analysis of leaf tissue of Col-0 and CAX mutants under standard growth conditions via ICP-MS of Na, Mg, Al, K, Ca, P, S, Cr, Mn, Fe, Co, Ni, Cu, Zn, As, Se, Mo, Cd, Sb and Pb (expressed as mg/kg dry weight) showed statistically significant differences for Mg, K, Ca, Mn, Fe, Cu and Zn (Figure 3A). When lines were arranged by increasing number of CAX mutations (Col-0, *cax1*, *cax3-1*, dKO, tKO and qKO) Mg, K, Ca, Mn, and Zn declined and Cu increased. Fe did not appear linked to the number of CAX mutations. Leaf Ca concentrations showed the strongest response to CAX mutation (F=31.2, p<0.0001): Ca concentrations in qKO were 58% of Col-0.

Elemental images of *cax1* (Supplemental Figure 4) agree with the bulk elemental data; changes in Ca in *cax1* are subtle in comparison with qKO. Distributional differences between *cax1* and Col-0 are seen in increased K, higher Ca abundance of the trichomes, and increases in the Zn in the (putative) guard cells. Abundance differences manifest as slightly lower Ca abundances in the vasculature. This is shown alongside the abundance and distributional changes observed in qKO for scale, which were more striking. Elemental images of dKO (Supplemental Figure 5), showing partial leaf section from mid-vein to the margin imaged alongside Col-0 in the same map, show greater abundances of Ca in the trichome and more Zn in the stomatal pores in dKO than Col-0.

Elemental images of qKO leaves imaged alongside size-matched Col-0 leaves are shown in Figure 3B. We observed differences in the distribution of K, Ca, Mn, Zn and Cl between Col-0 and QKO. Specifically, we observed more K in vasculature; more Ca, and Mn in trichomes, more Zn in guard cells and more Cl in vasculature. The similarity of dKO to the qKO image is

noted in this tricolor image, showing Ca, Zn and K. We observed slightly higher Ca abundances in the trichomes and strikingly higher Zn in putative guard cells in comparison with the coimaged Col-0 leaf. To explore differences in the trichome further, abundances of elements of Col-0 and qKO trichomes were extracted from elemental images by summing XRF spectra from user-defined regions and generating descriptive statistics from those areas (Figure 3C,D). We chose 5 trichomes at random from Col-0 and qKO leaf elemental images for comparison and expressed the data on a per pixel basis, and then conducted ANOVA statistical analysis. This showed that Ca and Mn were significantly higher in qKO compared to the Col-0 leaf, and Cl – although not statistically significant – showed the same pattern (Figure 3E).

Proteomic Analysis of Col-0, cax1 and qKO

199

200

201

202

203

204

205

206

207

208

209

210

211

212

213

214

215

216

217

218

219

220

221

222

223

224

Proteomic analysis gives insight into the molecular mechanisms responsible for the phenotypic differences observed between Col-0, cax1, and qKO leaf samples under normoxia conditions. This study identified a total of 1039 proteins from the three genotypes under study at a protein threshold with a probability of over 99% with at least two unique peptides (>95% probability) (Figure 4A). Of these proteins, 169, 25, and 58 were detected only in Col-0, only in cax1, or only in qKO, respectively (Figure 4A). Protein abundance was quantified using normalized spectral abundance factor (NSAF). Principle component analysis suggests that there are differences between the proteomes of the mutants compared to Col-0 (Figure 4B). Comparative studies of the protein abundance between the mutants and Col-0 are presented in detail in Supplemental Table 1, 2A, 3. Compared with Col-0, there are 164 and 70 proteins significantly decreased or increased respectively, in both cax1 and qKO. GO enrichment analysis of these proteins highlighted a greater primary metabolic process in Col-0, as showed by the significantly enriched categories including pyruvate metabolic process and starch metabolic process, which was supported by a higher apparent rate of photosynthesis in this line when compared to either cax1 or qKO (Figure 4C). The observed phenotypes of cax1 and qKO under normoxia conditions (Figure 1) may be

related to suppressed amino acid and fatty acid metabolic processes as highlighted by enrichment of these GO terms in the proteins which increased in abundance (Figure 4B). The mutants also showed enrichment in ribosome biogenesis and response to cold and oxidative stress (Figure 4C). This was supported by the higher abundance of proteins that have oxidoreductase and antioxidant activity (Supplemental Table 2B). The proteomic study also suggested a possible physiological mechanism for the mutant to tolerate abiotic stress. When comparing qKO with Col-0 alone, we found that a large number of proteins involved in chloroplast-localized electron transfer were significantly higher in qko (AT4G03280, AT4G03280, AT3G15640, ATCG00540, ATCG01060, AT4G23890) (Supplemental Table 2A, Supplemental Figure 6A), even though there was an overall apparent impairment of photosynthetic capacity in this line. To cope with the large number of electrons leaking from the ETC and generating an excess of ROS, the mutants may have evolved a stronger sensing and removal system for ROS, such as higher abundance in superoxide dismutase (AT5G18100, AT4G25100), which was also characterized as increased in abundance in cax1 even though not as pronounced as qKO (Supplemental Table 3). This was in line with our recent report that the cax mutants appear primed for the stress by having heightened expression of ROS related transcripts (53). Furthermore, the oxidative stress induced by ROS may cause the degradation of proteins including those with metal binding activities (37). This is consistent with a decreased abundance of proteins with metal binding activity (Supplemental Table 2, Supplemental Figure 6B).

245

246

247

248

249

250

225

226

227

228

229

230

231

232

233

234

235

236

237

238

239

240

241

242

243

244

Anoxia phenotype of plants lacking multiple Cation/H⁺ Exchangers

Every mutant combination that included *cax1* was tolerant to anoxia (Figure 7; Supplemental Figure 15). Tolerance to anoxia increased if an additional *CAX* gene was impaired. *cax1/2*, *cax1/3* and *cax1/4* lines showed similar anoxia tolerance (Supplemental Figure 15A,B). The tKO and qKO lines appeared more tolerant than dKO. The qKO and tKO lines displayed anoxia

tolerance even after 20h of treatment, whereas *cax1* lost its tolerance after 15 h (Figure 7A and Supplemental Figure 15C). The response to anoxia, while visually different between tKO and qKO, could not be resolved from chlorophyll measurements following anoxia (Figure 7A,B and Supplemental Figure 15B). Further, higher anoxia tolerance of the double, triple and quadruple mutants was linked to their decreased ROS accumulation, confirmed by 3,3'-diaminobenzidine (DAB) staining (Figure 7C).

Anoxia Phenotype of Plants Grown in Limiting Calcium Conditions

Previous work has established that cax1/3 mutants (dKO) have improved growth in low-calcium conditions compared to wild-type plants, and elemental analysis here demonstrates that sequential removal of CAXs reduces calcium content in leaf tissue. We posit that reduced calcium content may be a mechanism by which wild-type plants tolerate anoxia stress and thus sought to grow Col-0 in low calcium media (LCM) and access anoxia tolerance. Unlike Col-0 grown in standard conditions (166 mg/l CaCl₂), Col-0 grown for three weeks in LCM (22 mg/l CaCl₂) displayed anoxia tolerance like the CAX mutants (Figure 8).

RNAseq Analysis of *CAX* Mutants before, during and after Anoxia. We showed differential gene expression between the anoxia-sensitive (Col-0, *cax3*) and tolerant (*cax1*) lines (53). To determine how CAX transport contributes to tolerance, dKO and qKO were subject to RNAseq. The leaves of 21-day-old plants (9-rosette leaf stage) were harvested at the start of the treatment (0-hr control-pre), after being in the anoxia chamber for 4-hr (anoxia) and 1-hr post 7-hour anoxia treatment (post-anoxia). Each library consisted of at least 38 million reads (>94%) mapped to the Col-0 genome. RNAseq analyses were done for Col-0, *cax1(53)* and dKO before, during and after anoxia and qKO before and after anoxia (Figure 5). Treatments and mutants clearly clustered separately in principal component analysis (PCA) showing the first

and second PCs which together explained 52% of variances, suggesting the RNAseg was revealing differences between responses in the various genotypes (Figure 5A). Similar to our previous analyses (Col-0, cax3 and cax1,(53)), a large number of genes responded significantly during and after anoxia. 3099 genes were up-regulated in Col-0 during anoxia while 4879 genes were down regulated (Supplemental Table 4,5). The gene ontology (GO) categories for upregulated genes included cellular response to oxygen (Supplemental Figure 7A) and downregulated genes includes those involved in photosynthesis (Supplemental Figure 7B). Post-anoxia, 3638 genes were up-regulated with GO categories for cellular response to hypoxia (Supplemental Figure 8A, Supplemental Table 6) and 2873 genes downregulated representing GO categories related to photosynthesis (Supplemental Figure 8B. Supplemental Table 7). Having RNA-seq libraries from dKO and gKO allows further inferences to be drawn on the role of cation/H⁺ exchange in anoxia tolerance. We hypothesized that enhanced expression or repression of specific genes prior to the stress primes cax1 for anoxia. which confers tolerance (53). During normoxia, cax1 (1123 genes), dKO (1480) and qKO (820) lines had heightened expression of genes related to defense, oxidative stress, and programmed cell death (Figure 5B, C, Supplemental Table 8-10). We found that approximately 10% (116/1123) of the genes expressed at higher levels in cax1 during normoxia were expressed in Col-0 during anoxia (Supplemental Figure 9A). This increases in dKO and gKO: approximately 13% (192/1480) in dKO and 40% (320/820) in gKO (Supplemental Figure 9A). The same trend is observed with genes highly expressed in mutants during normoxia compared to Col-0 postanoxia (cax1: 61/1123-5%; dKO: 308/1480-20%; qKO: 426/820-51%) (Supplemental Figure 9C). Enriched GO categories for the up-regulated genes in qKO normoxia that were upregulated in Col-0 during anoxia and post-anoxia are clearly related to hypoxia (Figure 5F, G, Supplemental Table 11). When cax1 and dKO are included in the analysis, the GO terms are response to oxidative stress, secondary metabolic biosynthesis and defense (Supplemental Figure 9E ,F, Supplemental Table 12).

276

277

278

279

280

281

282

283

284

285

286

287

288

289

290

291

292

293

294

295

296

297

298

299

300

We also analyzed the down regulated genes among the CAX mutants in normoxia conditions and few commonly shared down regulated genes were found (Supplemental Figure 10A, Supplemental Table 13). However, many genes downregulated in the mutants during normoxia were downregulated in Col-0 during anoxia (*cax1*: 7/57-12%; dKO: 192/563-34%; qKO 17/48-35%) with a smaller percentage of overlap in down regulated genes with Col-0 post-anoxia (*cax1*: 3/57-5%; dKO: 136/563-24%; qKO 6/48-12.5%) (Supplemental Figure 11, Supplemental Table 14-16).

During anoxia, compared to Col-0, *cax1-1* (*cax1* throughout the remainder of the manuscript) and dKO both expressed 195 genes that were related to photosynthesis, response to light intensity, hydrogen peroxide and carbohydrate catabolic process (Figure 5D,E, Supplemental Table 17). During anoxia, 361 genes related to defense, organ senescence and response to salicylic acid were down regulated in *cax1* and dKO (Supplemental Figure 10B,C, Supplemental Table 18). Post anoxia, dKO and qKO both expressed 42 genes related to photosynthesis and defense that were not expressed in Col-0 (Figure 5H,I, Supplemental Table 19). Post-anoxia qKO repressed 525 genes in comparison to Col-0, many of these involved in hypoxia responses and hormone signaling (Supplemental Figure 10D,E, Supplemental Table 20). 193 genes repressed in both qKO and dKO appear to be involved in long-chain fatty acid metabolism, response to water, and stomatal function (Supplemental Figure 10D,F, Supplemental Table 21).

We mined the expression data for increased or decreasing expression of genes highly responsive to Ca/H, depending on the number of CAX mutants (*cax1*>dKO>qKO and qKO>dKO>*cax1*). From 128 common upregulated genes during normoxia (Figure 5B), 20 fit the expression pattern of *cax1*>dKO>qKO (these genes are related to regulation of development and root morphogenesis) (Supplemental Figure 12A,B and Supplemental Table 22) and 6 qKO>dKO>*cax1* (Supplemental Figure 12C, Supplemental Table 23). None of the down-regulated genes fit the pattern of *cax1*>dKO>qKO.

Ca signaling in CAX mutants during reoxygenation

328

329

330

331

332

333

334

335

336

337

338

339

340

341

342

343

344

345

346

347

348

349

350

351

352

353

Given that CAX1 is highly expressed in leaves, it could be the primary H⁺/Ca exchanger involved in post-anoxia Ca signaling in the aerial portion of the plant (40). Previous work demonstrates that Ca signals are significantly different between the anoxia-tolerant cax1 and sensitive Col-0 during reoxygenation(53); here we aim to identify if CAX3 (dKO vs cax1) and CAX4 (dKO vs tKO) influence leaf Ca signaling post-anoxia. Stable transgenic lines of dKO and tKO expressing cytoplasmic GCaMP3 (a GFP based Ca biosensor;(53)) were used to visualize the progression of Ca signals in the cytoplasm following anoxia and wounding (supplemental movies 1 and 2). The mutants showed no changes during wounding but re-oxygenation after exposing the plants to 4h of anoxia treatment displayed differences in the temporal signals produced in the double and triple mutants, compared to the cax1 single mutant. In the older leaves (first pair of true leaves/leaf 1) of dKO and tKO, a strong initial signal peaked at around 100 sec (111 and 125 sec for dKO and tKO, respectively), compared to the first signal at 201 sec in cax1 (Figure 6A.B. Supplemental Figure 13A,B, Supplemental Movie 1,2); the dKO and tKO lines are similar, suggesting that CAX4 has a minimal role in this response. However, the response in these mutants is different than cax1 and Col-0, highlighting the importance of CAX3.In most cases, fluorescence intensity was found to be higher in both dKO and tKO (Supplemental Figure 13A). In the younger leaves (leaf 3), the Ca signal peaked at around 100 sec and was present in all the mutant genotypes with slight variation in the intensity (Supplemental Figure 13A). This suggests that CAX3 and CAX4 have a limited role in post-anoxia Ca signaling in these leaves. As shown previsly (53), older Col-0 leaves had a prominent initial Ca signal, which dissipated in the first 50 sec (Supplemental Figure 13A) and a second minor signal after 150/160 sec. The pattern was similar in the younger leaves, but with lower fluorescence intensity (Figure 6A,B and Supplemental Movie 1,2). A clear signal was present in the meristematic region in all the genotypes, during the entire imaging interval (6 minutes). A drop in the intensity was observed at around 100 sec in all genotypes (Figure 6A,B, Supplemental Movie 1,2). This suggest that in the

meristem, the CAXs have a minor role in shaping the Ca signal post-anoxia. We ensured that the changes in the calcium dynamics in the CAX mutants are specific to anoxia stress by analyzing the calcium signals in these genotypes following wounding (Supplemental Figure 14A,B). All four genotypes showed a similar movement of the cytoplasmic calcium. Mostly, the signal was limited to the leaf in which the stress was induced meaning it does not produce calcium changes at a whole plant level (Supplemental Figure 14A). All these plants showed a gradual increment in the intensity following wounding, which peaked between 50-80 sec and reduced afterwards (Supplemental Figure 14B). Additionally, we did not observe any statistically difference in the Ca signals between Col-0 and *cax* mutants during normoxic conditions (Supplemental Figure 14C), further confirming that the sensor is working in the same way in different genotypes.

Discussion

This work characterizes plants lacking all four functional CAX transporters and provides new data regarding cax1/3 (dKO). Concurrently, this work compares some phenotypes obtained from cax1 and cax1/3 lines. It also further defines the role of specific transporters. Single and double mutants partially impair transport: a 50% reduction in *cax1* and 53% in dKO (9); here qKO demonstrated at least an 85% reduction demonstrating that in these conditions, CAX2 and CAX4 have a prominent role in transport (Figure 2). This quadruple mutant has pleiotropic phenotypes and allows an unparalleled biological resource to discern the role of high-capacity low-affinity tonoplast localized H⁺/Ca transport in plant signaling and elemental repartitioning (Figures 3, 4, 5,6,7).

Previous studies have demonstrated different transport properties and tissue localization of the CAXs (40; 41); this study continues to clarify the roles of these transporters. CAX1 and CAX3 (dKO) loss also appeared to be a tipping point for changes in Ca signaling and elemental distribution in leaves during normoxic conditions (Figure 3, 6); meanwhile, previous studies have

suggested CAX3 had a minimal role in calcium homeostasis in aerial tissues (34). Post-anoxia Ca signaling in leaf 1 changes more dramatically in the dKO and tKO lines than *cax1*, demonstrating that CAX3 impacts anoxia signaling through changes in Ca signaling (Figures 6). In the *cax1* background, each additional CAX mutation lowered calcium levels in the leaf tissue (Figure 3), altered leaf protein and gene expression (Figure 4,5), and increased anoxia tolerance (Figures 7). These phenotypes suggest all four CAXs can function in leaf tissue.

Plant calcium signaling is a complex process with many transporters altering cytosolic calcium levels (45). The reduced tonoplast transport in qkO may increase Ca sequestration into other endomembrane compartments and cause changes in capacitative Ca entry (store-operated entry)(5; 17; 29): in qkO lines, ER and other endomembrane calcium stores might communicate a "filled state" to the plasma membrane to diminish endogenous Ca levels (Figure 2) and alter Ca signaling and nutrient sensing (46)(Figure 6). Alterations in CAXs impact proton pumps (11) and future work will need to be directed at determining how the drastic change in tonoplast calcium transport affects the dominant proton pumps such as the plasma membrane ATPase, the vacuolar pyrophosphatase (V-PPase), and the vacuolar-type ATPase (V-ATPase).

The altered transport in the qKO mutants (Figure 2) impacted changes in elemental abundance and distribution in leaf tissue (Figures 3). These changes were not seen in *cax1* and were not significantly altered by loss of CAX2 and CAX4. The most striking differences were in dKO and qKO were (1) remobilization of Ca to the trichomes, (2) increased Zn in what we assume are the guard cells and (3) increased Cl levels throughout the lamina and vasculature (Figure 3; Supplemental Figure 4). The characteristic punctate Zn distribution was a consistent observation in our leaf images. Because the CAXs do not appear to transport Zn, these images indicate that abolishing CAX-mediated transport affects Zn distribution. Published whole leaf Zn maps are scarce, but our previous study (25) analyzing altered Fe homeostasis displays a similar but less pronounced, punctate Zn phenotype.

Likewise, CI is not thought to be transported by CAXs, nor has it consistently been measured in studies of the CAXs, but was perturbed in qKO, which had more CI in the trichomes (Figure 3E). Chlorine may play a pivotal role in osmotic regulation (15), and this perturbation could indirectly result from CAX deletion. The SXRF observations indicate a cascade of changes resulting from a change of CAX-mediated transport, underscoring the multi-elemental interplay when biological systems are perturbed and the advantages of taking a multi-elemental analytical approach.

Bulk concentrations of Ca in qKO leaves were lower than wild-type, *cax1*, dko, and tKO, as were Mn, Mg, K, and Zn, although to lesser extents (Figure 3). However, these quantitative changes were less apparent in the elemental imaging. Comparisons between spatially resolved and volume-averaged concentrations could be more intuitive. They should be made cautiously: bulk analysis averages out elemental concentrations across the whole shoot biomass of many plants, whereas elemental images focus on a single leaf at the micron scale, and trends area function of scale. Higher abundances of Ca in the trichome of qKO (Figure 3E) cannot be extrapolated to an increase in Ca abundance of the entire shoot biomass, as much as it indicates a remobilization of Ca.

In qKO Ca abundance was higher in the trichomes (Figure 3E); a significant storage location for metals in various flowering plant species. Trichomes have long been known as a mineral storage location for plants (44). Some hyperaccumulator species store potentially toxic, non-essential metals and Ca in trichomes (7). Mutants in CAX1 are tolerant to serpentine soils (6) and Cd stress (3), and the altered metal distribution or elemental abundance documented here may help explain these phenotypes (52).

The sequential disruption of CAX transport allows a more thorough examination of the role of Ca/H disruption in anoxia tolerance: anoxia tolerance is not due to the loss of specific transport properties of CAX1. If this were the case, the dKO, tKO, and qKO lines would be equally

tolerant to anoxia as cax1. Anoxia tolerance is probably not caused by changes in apoplastic free Ca levels, because this is a dKO phenotype (and presumably also present in tKO and qKO) not seen in cax1 (16). Furthermore, stomatal movement and phosphate homeostasis are unaffected in cax1 (13; 32), suggesting that anoxia tolerance does not result from these changes. A knockout of CAX1 in Arabidopsis alters tolerance to various metals, Ca-depleted conditions, and freezing after cold acclimation (2; 3; 6; 10). We posit these phenotypes are caused by altered Ca, or pH homeostasis at the tonoplast (11) and, given the modified transport properties observed here, will be more robust in dKO, tKO, and qKO. The CAX mutants may have numerous adaptations that allow them to endure anoxia stress (53): an essential component of this tolerance could be decreased internal calcium levels and the constitutive expression of a suite of anoxia tolerance genes (Figures 5,7). This work demonstrates that during normoxia, qKO had elevated expression of approximately 40% of the genes Col-0 expresses at high levels during or post-anoxia. Many of these genes are involved in defense. but some are involved in hypoxia responses (Figure 5F,G, Supplemental Table 11). Similar comparisons using dKO, while not as dramatic as those with qKO, further support the idea that CAXs mutants may be anoxia tolerant due to changes in gene expression present before anoxia stress. In agreement with this, qKO also showed changes to cellular redox homeostasis at the proteomic level, with increased abundance in enzymes involved in ROS production and removal when compared to Col-0 (Supplemental Table 2) (38). The mutants are primed for anoxic conditions, as the proteomic analysis indicates that the absence of CAXs already imposed stresses, which was reflected by reduced growth which we posit is caused by changes in carbon fixation and carbohydrate metabolism (Figure 1,4). Given that wild-type plants grown in reduced calcium-containing media is anoxia tolerant (Figure 8), it will be interesting to determine if these growing conditions impact the expression of stress genes and elemental partitioning. The loss-of-function of CAXs – diminishing Cation/H+ exchange – appears to have

adaptive advantages, with a "less is more" phenotype regarding Cation/H+ exchange activity

430

431

432

433

434

435

436

437

438

439

440

441

442

443

444

445

446

447

448

449

450

451

452

453

454

and anoxia tolerance (Figure 1,4) (53). Loss-of-function alleles were once the epitome of deleterious genetic variation (27). This study further appreciates the reduction of CAX activity as an adaptation to plant stress (2; 6; 10; 36). It will be interesting to survey various plants to delineate if diminished CAX function and changes in calcium content increase stress tolerance (14; 21); if such plants exist, how do they compensate for impaired CAX function during normal growth conditions?

Materials and Methods

Plant Materials and Growth

Arabidopsis wild-type (Col-0) and *CAX* mutant seeds (*cax1-1*, cax3-1, *cax1-1/cax3-1* double mutant, *cax1-1/cax2-2* double mutant, and *cax1-1/cax4-1* double mutant, *cax1-1/cax3-1/cax4-1* triple mutant and *cax1-1/cax2-2/cax3-1/cax4-1* quadruple mutants were used in the study. All these mutants were genotyped to confirm the presence of T-DNA insertions (Supplemental Figure 16 and Supplemental Table 24). The seeds were surface sterilized in 20% bleach and grown on half-MS medium (Murashige and Skoog; Sigma), or LCS (16) containing 0.5% sucrose and 0.7% agar with a modest addition of CaCl₂ (LCM-22mg/l) and were incubated at 12 h light, 22°C, and 12 h night 20°C. For morphological analysis, plants belonging to 2 rosette leaf stage (Boyes et al 2001) were transferred to soil and grown at 12 h light, 22°C, and 12 h night 18°C. For checking the Ca²⁺ ion sensitivity of the various mutants, 5-days old plants (cotyledon stage) were transferred to half-MS medium supplemented with 25mM CaCl₂. Growth characteristics were observed 15 days after their transfer to the altered media.

Anoxia Experiments

For anoxia experiments, 21 days old plants (9 rosette leaf stage) grown under the abovementioned conditions were placed in a AnaeroPack system (Mitsubischi Gas Chemical) anaerobic atmosphere generation bags (Sigma) with one CampyGen 3.5L bag (Thermo Scientific). The surgical tapes around the plates were removed prior to keeping them in the system. The experiment was performed for 10h unless mentioned otherwise. Experiments were usually done in the nighttime. After the anoxia treatment, plants were returned back to the growth chamber. Images were taken after four days using a Nikon D80 Digital SLR Camera (Nikon Corp., Tokyo, Japan).

Chlorophyll fluorescence measurement.

Chlorophyll estimation was performed as described previously (31). Briefly, 50mg of tissue form both pre-anoxia and post-anoxia samples were ground in liquid nitrogen and a homogenate was prepared in 80% acetone. After centrifugation, supernatant was collected, and the pellet was reextracted with 80% acetone. The extraction process was repeated three times until the pellet became colorless. After pooling, absorbance of the supernatant was measured at wavelengths 645 and 663 nm with a Cary 50 spectrophotometer. Measurement of chlorophyll a, chlorophyll b and total chlorophyll was estimated using Arnon's equation (1). Plants belonging to 9-rosette leaf stage were used for the experiment and the whole rosette were isolated 24h after anoxia treatment. Each experiment was carried out with 3-4 replicates, and the whole experiment was replicated four times. Statistical significance was calculated using Student's t-test and ANOVA.

Combined patch-clamp and fura-2 fluorescence experiments

The Arabidopsis mesophyll protoplast isolation procedures and vacuole release were described elsewhere (23). Patch-clamp recordings were performed in the whole-vacuole configuration using a List Medical amplifier and Pulse acquisition software (HEKA Electronic, Germany). Isolated vacuoles were observed using a 40× oil objective (overall magnification 400×) mounted on an inverted Axiovert microscope (Zeiss, Germany). Patch pipettes were pulled from thin-walled

borosilicate glass capillaries (Harvard Apparatus, USA) and had final resistances of 2-3 MΩ with standard pipette solution containing (in mM): 100 KCl, 3 MgCl₂, 0.4 EGTA, 20 bis-tris-propane, 230 D-sorbitol, pH 7.0 (with MES) and 500 mOsm, supplemented with 100 µM fura-2 pentapotassium salt. The standard (cytosolic) bath solution contained (in mM): 100 KCl, 3 MgCl₂, 2 EGTA, 5 HEPES, 280 D-sorbitol, pH 7.2 (with KOH) and 515 mOsm. Chemicals were purchased from Merck (Italy). The vacuole was held at a membrane voltage of -40 mV and continuously perfused with standard bath solution by a gravity-driven perfusion system coupled to a peristaltic pump (Gilson Inc., USA). For fura-2 detection, a monochromator (Cairn Research, UK) selected the excitation light generated by a Xenon arc lamp (Photon Technology International, USA), alternately at 340 nm and 380 nm in 100-ms excitation cycles. Fluorescence emission (F₃₄₀ for 340-nm excitation and F₃₈₀ for 380-nm excitation) was detected using a 515-nm bandpass emission filter and recorded every 300 ms by a CCD camera (Roper Scientific, Germany). Fluorescence signals were detected inside a region of interest (ROI) covering the vacuole. MetaFluor software (Molecular Devices, USA) was used to control the system and to calculate online the F₃₄₀/F₃₈₀ fluorescence ratio. Background fluorescence, measured in a ROI far from the vacuole, was subtracted off-line. After reaching the whole-vacuole configuration, vacuolar fura-2 loading required between 20 and 40 minutes. Thereafter, a calcium gradient between the cytosolic side and the vacuolar lumen was established by replacing the standard bath solution with a solution containing (in mM): 100 KCl, 3 MgCl₂, 5 Hepes, 280 D-sorbitol, pH 7.2 (with KOH) supplemented with 10 or 30 µM CaCl₂. The calcium contamination in the Ca²⁺-free solution was less than 2 µM, as determined by atomic absorption spectroscopy. Experimental conditions were carefully chosen such to exclude any major contribution to the vacuolar Ca²⁺ signals by two-pore channel 1 (TPC1), a highly abundant, calcium-activated vacuolar cation channel permeable to Ca2+ (22). In a series of control experiments on Col-0 and tpc1 knock-out plants, currents and fluorescence signals were monitored varying [Ca2+] and holding voltages.

506

507

508

509

510

511

512

513

514

515

516

517

518

519

520

521

522

523

524

525

526

527

528

529

530

For fura-2 calibration, fluorescence signals were determined in a 500-µl droplet of standard pipette solution placed onto the bottom of the recording chamber, supplemented with 5 mM EGTA ("zero calcium" condition) and 20 mM CaCl₂ ("saturated calcium" condition). The vacuolar free calcium concentration was then calculated according to the equation(24):

$$[Ca^{2+}] = K_d \left(\frac{R - R_{min}}{R_{max} - R} \right) \left(\frac{F_{380,max}}{F_{380,min}} \right)$$

where R is F_{340}/F_{380} , R_{min} is F_{340}/F_{380} at zero calcium, R_{max} is F_{340}/F_{380} in saturated calcium, is the ratio between F_{380} in zero calcium and F_{380} in saturated calcium; K_d , the dissociation constant of the dye at room temperature, is 224 nM (24).

Statistical analysis for Transport Data

Results are given as mean ± standard error (SE). For statistical analysis and graph preparation, Igor Pro (WaveMetrics Inc., USA) and Excel software (Microsoft Corp., USA) were used. Statistical significance was determined using Wilcoxon's Rank test.

RNA Extraction, transcriptomic analysis and Quantitative Real-Time qPCR.

(50mg) was ground in liquid nitrogen and homogenate was prepared in trizol. Following centrifugation, upper aqueous phase containing RNA was separated and precipitated with isopropanol. RNA was treated with Dnase to remove any contaminating DNA and the quality was assayed by Bioanalyzer.

For transcriptome analysis, RNA samples were outsourced to BGI Genomics (BGI Americas Corporation, Cambridge, MA, USA). RNA-seq was performed using DNBseq platform using 150 bp pair-end sequencing chemistry. A minimum of three independent replicates were used for each conditions analyzed. All the samples had a RIN value above 7. On average, sequencing yielded 38 million reads per sample. The raw reads were cleaned by removing the adapters and low-

Total RNA was isolated from 21days old plants (9-rosette leaf stage) with Trizol. Whole rosette

quality sequences. Trimmed reads were then mapped to the reference genome of *A.thaliana* obtained from The Arabidopsis Information Resource (TAIR)(TAIR10_Araport11_www.arabidopsis.org_20190423). On average more than 94% of the reads were mapped to the reference genome using STAR v2.7.6a (19). Assembly of RNA-Seq alignments into transcripts were performed using Stringtie2.1.5 (39). The differential gene expression were analyzed using edgeR and limma R libraries. RNA-seq data will be deposited in the SRA database with the accession no (pending).

Quantitative RT-qPCR was used to validate the RNA-seq data. Dnase treated RNA was converted into single-stranded cDNA using oligo dT18 primers (SuperScript™ First-Strand Synthesis System for RT-PCR, Invitrogen). For RT-qPCR, 10ng of the cDNA was used. The quantification was done with iTAQ SYBR Green Master Mix (Bio-Rad) in Biorad CFX96 Real-Time PCR System (Biorad) with gene specific primers (Supplemental Table 25). The reaction consisted of 95°C for 30 sec, 40 cycles each of denaturation at 95°C for 5 sec and annealing and extension at 60°C for 30 sec followed by additional cycle of 65°C for 5 sec and 95°C for 5 sec. The expression was normalized to Arabidopsis UBQ10 and the fold changes were calculated by 2-ΔΔCt method. Statistical significance was calculated by Student's T test in Excel (Supplemental Figure 17).

Protein isolation, Mass Spectrometry and Protein Identification and Quantification.

Whole rosettes from 6-rosette leaf stage plants were used for protein extraction (4)Barkla et al Plant cell 2009). 3g of the tissue was ground in liquid nitrogen and were homogenized in prechilled extraction buffer (100 mM Tris-MES, pH 8.0, 1 mM EGTA, 5 mM dithiothreitol, 4 mM MgSO4, 5% [w/v] insoluble PVP, and plant protease inhibitor cocktails (Sigma Aldrich, St. Louis, MO) to the recommended concentration by manufacturer). The total proteins in supernatant (500 μ L) were then precipitated using 200 μ L 10X TE, 200 μ l of 0.3% sodium deoxycholate, and 200

582 µl of cold 72% TCA. The protein pellets were washed in 90% methanol at room temperature and 583 subsequently lyophilized. Cellular debris were removed by first filtering through Miracloth 584 (Calbiochem, La Jolla, CA), and clarifying by centrifugation. 585 Protein identification was carried out at the Institute for Molecular Biosciences proteomics facility 586 at the University of Queensland, Brisbane. Proteins were analysed using an Eksigent, Ekspert 587 nano LC400 uHPLC coupled to a TripleTOF 6600+ System (SCIEX, Canada) equipped with a 588 PicoView nanoflow ion source (New Objective, USA). Protein extract (up to 5 µI) was injected 589 onto a ChromXP C18-CL column (3 µm, 75 µm x 150mm) (SCIEX, Canada). Peptide elution was 590 carried out running linear gradients of 5-30% solvent B (0.1% formic acid in acetonitrile) over 120 591 min at 400nL/minute flow rate, followed by 30-90% solvent B for 3 min, and 90% solvent B for 17 592 min and was returned to 5% solvent B for equilibration prior to the next sample injection. Mobile 593 phase used consisted of solvent A; 0.1% formic acid in water, and solvent B; 0.1% formic acid in 594 acetonitrile. Following conditions were used for the experiment; column temperature was 595 maintained at 45°C, ion spray voltage was set to 2600V, declustering potential at 80V, curtain gas 596 flow 25 psi, nebuliser gas 30 psi, and interface heater at 150°C. The mass spectrometer was set 597 to acquire 100ms of full scan TOF-MS data over the mass range 350-1500 m/z, followed by up to 598 fifty 50ms full scan product ion data in IDA mode over the mass range 100-1500 m/z. Ions 599 observed in the TOF-MS scan exceeding a threshold of 100 counts and a charge state of +2 to 600 +5 were set to trigger the acquisition of product ion MS/MS spectra of the resultant 50 most 601 intense ions. Protein Pilot 5.0.2 (SCIEX, Canada) was used to search spectra against the Uniprot 602 Arabidopsis database (proteins, May/12/2020) and encode the output mzldentML file for the 603 downstream analysis. Scaffold 4.8.6 (Proteome Software, Portland, OR, USA) was used to 604 validate MS/MS-based protein identifications and quantification. Protein identifications were 605 accepted if they could be established at greater than 99% probability and contained at least two 606 unique peptides. Normalized spectral abundance factor (NSAF) was used for protein 607 quantification (Gulcicek et al, Curr Protoc Bioinformatics, 2005; and Searle, Proteomics, 2010)

Proteins identified in at least 2 out of 3 biological replicates were considered as present in the corresponding genotypes. To evaluate the significance of comparative quantification by different genotypes, Student's t-test was performed on the data, and the differences were assigned to be significant at a p-value less than 0.05. Differentially abundant proteins (DAPs, including exclusively present proteins) were submitted to David Bioinformatics Resources 6.8 for Gene Ontology enrichment analysis (Huang, Nat Protocol, 2009).

614

615

616

617

618

619

620

621

622

623

624

625

626

627

628

629

630

631

632

608

609

610

611

612

613

Real-time measurements of cytosolic Ca in plant leaves post anoxia

CAXs mutants harboring GCaMP3 sensor (a GFP based Ca indicator) were generated by crossing the mutants with Col-0 plants harboring GCaMP3 sensor. Homozygous lines generated in subsequent generations were confirmed by genotyping. Col-0, cax1-1, cax3-1, cax1/3/4 harboring GCaMP3 sensor were surface sterilized in 20% bleach and grown on half-MS medium (Murashige and Skoog; Sigma), containing 0.5% sucrose and 0.7% agar at 21°C till they reached the 5-rosette leaf stage. On the day of imaging experiment, individual plate was foil covered and transferred to a vacuum sealer bag (Wevac) with 1 CampyGen 3.5L bag (Thermo Scientific) for 4 h. A folded layer of tissue paper was placed between the bag and the plate to avoid any heat stress. GCaMP3 fluorescence were measured immediately after re-exposing the plates to oxygen with a motorized fluorescence stereo microscope (Zeiss Axio Zoom V16) equipped with a PlanApo Z 1.0× objective lens and a Zeiss AxioCam HRm sCMOS camera. GCaMP3 was excited using a mercury lamp (Zeiss HXP 200c Illuminator), with a 470/40 nm excitation filter, and a 500 nm dichroic mirror. The green fluorescent signal passing through a 535/50 nm emission filter was acquired every 1 s with the using Zeiss Zen pro imaging software. Fluorescence in the entire first true leaf over time were converted into signal values using ImageJ. A similar sized background was identified and the mean fluorescence over time was subtracted to obtain the actual leaf fluorescence value.

Experiments were run in duplicate each day and experiments repeated on different days over the course of multiple months until data from at least 5 replicates was recorded. Statistical analyses were performed with ANOVA and Tukey's post-hoc testing or the student T-Test formula in Microsoft Excel. Significance was set at P < 0.05. Data were presented as means ± SEMs.

ICP-MS

Samples of shoot tissue were acid digested by closed vessel microwave assisted digestion; 1 ml of HNO₃ and 0.1 ml HCl was added to 25 mg of sample and the digestion temperature ramped to 95°C over 15 minutes and held for a further 45 minutes. Following digestion samples were diluted to 10 ml with deionized water. Digested samples were analyzed by collision cell inductively coupled plasma mass spectrometry (ICP-MS) (Agilent, 8900) operated in helium gas mode. Quality control included initial and continuing calibration checks, 3 replicate digestion duplicates, spikes and standard reference materials (SRMs) (NIST 1515, Gaithersburg, MD), analysis duplicates and analysis spikes. Method detection limits and standard reference material recoveries (%) are given for all elements in Supplemental Table 26.

Statistical Analysis

After establishing normality, we conducted one-way analysis of variance (ANOVA) on non-normalized metal concentration data, with data below detection limits assigned a missing value. Means comparisons were conducted using Tukey's statistical tests. Statistical analysis was conducted in JMP version 16.0.

SXRF elemental imaging

Elemental images of leaves were collected at the 4-BM XFM 3-pole wiggler imaging beamline of the National Synchrotron Light Source-II (NSLS-II) (Upton, NY). XFM has an energy range of 2.3-23 keV, with a flux of ~2 x 10¹¹ photons/sec (for the Si(111) monochromator). Energy

resolution was $\sim 10^{-4}$ ($\Delta\lambda/\lambda$). Our experiments were conducted at 10 keV (optimized for the analysis of Ca), at 10 µm resolution (10 µm beam, 10 µm step) and 50 millisecond dwell using polychromatic 'pink-beam' mode for rapid imaging. XFM used a Hitachi Vortex ME4 silicon drift detector.

Plants were maintained on solid media in a Conviron[™] growth chamber at 22°C with 16/8-hour light/dark cycles until analysis. Leaves were cut from actively growing plants with micro scissors immediately before analysis and adhered to single-sided Kapton metal-free tape stretched across custom 35 mm acrylic stage mounts. A size-matched Col-0 leaf was included in each map of transgenic lines for relative abundance comparison. For faster (exploratory) scanning, half of the leaf was scanned at the mid-vein, and full maps were collected from entire leaves, avoiding the cut-edge of the petiole. Mounting times were less than 5 minutes. For shorter maps (500 pixels²) scan times were approximately 4 hours, and larger maps scan times were approximately 11 hours.

Quantification of normalized fluorescence count data into ppm was conducted using National Institute of Standards and Technology (NIST) standard reference material (SRM) 1833 and 1832. Neither of these SRMs have a certified value for chorine. Data was visualized using GSE CARS Map Viewer software, which allows user-defined region of interest analysis of elemental maps. This was used to compare elemental abundances of lamina and trichomes between transgenic lines.

Accession Numbers

Sequence data from this article can be found in the GenBank/EMBL data libraries under accession numbers

- 685 Supplemental Data
- Supplemental Figure 1. Enhanced Growth of dKO, tKO, and qKO compared with Col-0,
- 687 cax1 and cax3 mutants.
- 688 Supplemental Figure 2. Notable phenotypic differences between cax1 single mutants and
- 689 dKO, tKO and qKO.
- 690 Supplemental Figure 3. Fura-2 reports luminal calcium increases in isolated vacuoles.
- 691 Supplemental Figure 4. Scaled quantified elemental images collected via synchrotron X-
- ray fluorescence of cax1 and qKO leaves imaged alongside size-matched Col-0.
- 693 Supplemental Figure 5. SXRF elemental images of size-matched Col-0 and dKO mutant
- 694 leaves.
- 695 Supplemental Figure 6. GO enrichment analysis of the proteomic study.
- Supplemental Figure 7. GO biological pathways of differentially expressed genes in Col-0
- 697 during anoxia.
- Supplemental Figure 8. GO biological pathways are differentially expressed genes in Col-
- 699 **O post-anoxia**.
- 700 Supplemental Figure 9. Up-regulated Genes shared by Col-0, cax1, dKO and qKO.
- 701 Supplemental Figure 10. CAXs mutants transcriptome-wide responses to anoxia.
- 702 Supplemental Figure 11. Downregulated genes shared by Col-0, cax1 and dKO and qKO.
- 703 Supplemental Figure 12. From 128 common upregulated genes in cax1, dKO, qKO
- 704 normoxia.
- Supplemental Figure 13. Calcium changes in Col-0, cax1, dKO and tKO during exposure
- 706 to oxygen after anoxia stress.
- 707 Supplemental Figure 14. Changes in the cytosolic calcium signals in selected CAX
- 708 mutants during wounding (A and B) and in normal environmental/normoxic conditions
- 709 **(C)**
- 710 Supplemental Figure 15. Anoxia phenotype of plants lacking multiple CAXs.

- 711 Supplemental Figure 16. Genotyping CAXs mutants.
- 712 Supplemental Figure 17. Validation of RNA-seq data by RT-qPCR.

- Supplemental Table 1. Comparative studies of the protein abundance between Col-0 vs
- 716 cax1.
- 717 Supplemental Table 2A. Comparative studies of the protein abundance between Col-0 vs
- 718 **qKO**.
- 719 Supplemental Table 2B. Comparative studies of the protein abundance between Col-0
- 720 and mutants in normoxic conditions.
- 721 Supplemental Table 3. Comparative studies of the protein abundance between *cax1* vs
- 722 **qKO**.
- 723 Supplemental Table 4. Genes highly up regulated in Col-0 during anoxia.
- 724 Supplemental Table 5. Genes highly down regulated in Col-0 during anoxia.
- 725 Supplemental Table 6. Genes highly up regulated in Col-0 post anoxia.
- 726 Supplemental Table 7. Genes highly down regulated in Col-0 post-anoxia.
- 727 Supplemental Table 8. Genes highly up regulated in *cax1* during normoxia.
- 728 Supplemental Table 9. Genes highly up regulated in dKO during normoxia.
- 729 Supplemental Table 10. Genes highly up regulated in qKO during normoxia.
- 730 Supplemental Table 11. Genes highly up regulated in qKO during normoxia, Col-0 during
- and post anoxia.
- 732 Supplemental Table 12. Genes highly up regulated in *cax1*, dKO, qKO during normoxia,
- 733 Col-0 during and post-anoxia.
- 734 Supplemental Table 13. Genes highly down regulated in cax1, dKO and qKO during
- 735 normoxia.
- 736 Supplemental Table 14. Genes highly down regulated in cax1 during normoxia.

- 737 Supplemental Table 15. Genes highly down regulated in dKO during normoxia.
- Supplemental Table 16. Genes highly down regulated in qKO during normoxia. 738
- 739 Supplemental Table 17. Genes highly up regulated in cax1 and dKO during anoxia.
- 740 Supplemental Table 18. Genes highly down regulated in cax1 and dKO during anoxia.
- 741 Supplemental Table 19. Genes highly up regulated in dKO and qKO post anoxia.
- 742 Supplemental Table 20. Genes highly down regulated in gKO post-anoxia.
- 743 Supplemental Table 21. Genes highly down regulated in dKO and qKO post-anoxia.
- 744 Supplemental Table 22. Genes with expression pattern of cax1>dKO>qKO.
- 745 Supplemental Table 23. Genes with expression pattern of qKO >dKO>cax1.
- 746 Supplemental Table 24. List of primers used for genotyping.
- 747 Supplemental Table 25. List of primers used for RT-qPCR validation.
- 748 Supplemental Table 26. Method detection and standard reference material recoveries.
- 749 Supplemental Movie 1. Calcium changes in Col-0, cax1 and dKO post anoxia.
- 750 Supplemental Movie 2. Calcium changes in Col-0, cax1 and tKO during wounding.

752 Funding This work was supported by grants to T.P. and K.D.H from the National Science 753 Foundation (1557890), and grants to K.D.H from USDA (3092-51000-061-00D) and National

754 Institute of Health (R03 Al149201-02). This research used beamline 4-BM of the National

755 Synchrotron Light Source, a U.S. Department of Energy (DOE) Office of Science User Facility 756

operated for the DOE Office of Science by Brookhaven National Laboratory under Contract No.

757 DE-AC02-98CH10886.

758

751

759 Acknowledgements: We thank Ardawna Green for help growing the plants. Simon Gilroy for 760

help establishing the calcium imaging procedures and Jon Pittman for reading an early version 761 of this work. This research used the X-Fluorescence Microprobe (XFM) beamline (4-BM) of the

762 National Synchrotron Light Source II, a U.S. Department of Energy (DOE) Office of Science

763 User Facility operated for the DOE Office of Science by Brookhaven National Laboratory under

Contract No. DE-SC0012704. 764

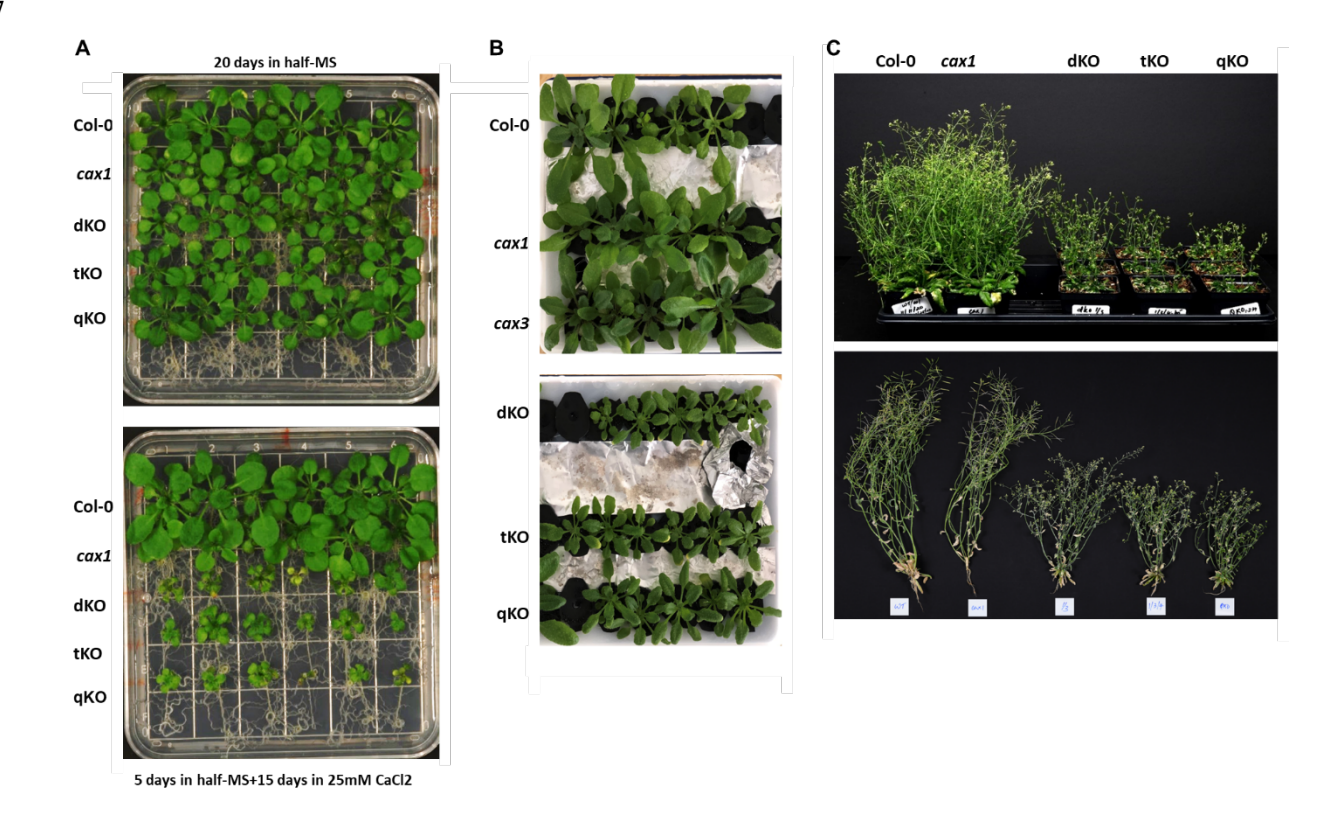


Figure 1. Growth characteristics of CAXs mutants. (A) Reduced growth of CAX mutants in media containing 25mM CaCl₂. Seeds were germinated and grown in half-MS medium for 15 days before they were transferred to medium containing calcium (lower panel). Photographs were taken 5 days after transferring to the supplemented medium. Control plants grown on half-MS medium for 20 days is given in the upper panel. (B) Reduced growth of CAX mutants in hydroponic basal nutrient solution (BNS) containing 1mM calcium. (C) Altered growth of dKO, tKO and qKO in soil. dKO, tKO and qKOs were much smaller than Col-0 and *cax1* single mutant. All these plants were grown on half-MS media for 10 days before transferring to soil.

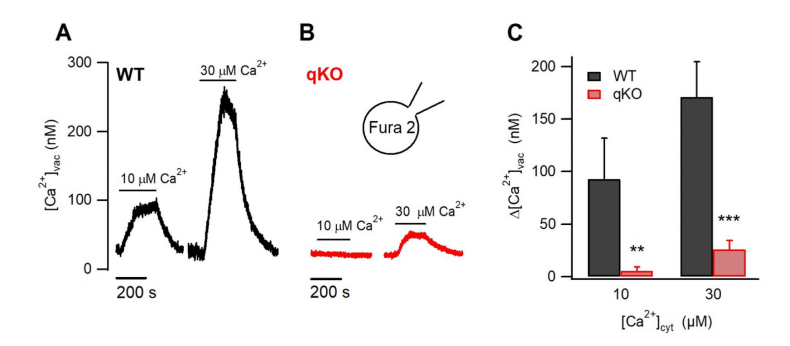
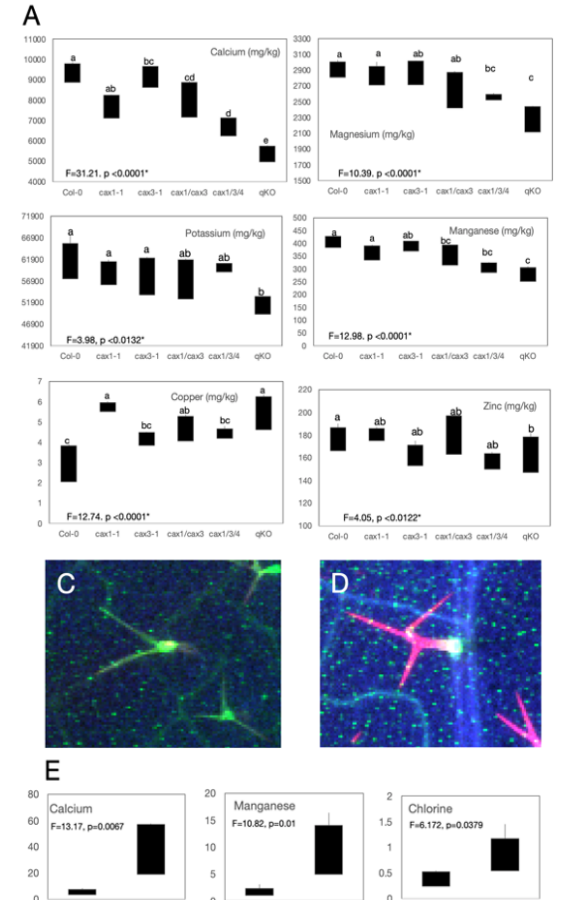


Figure 2. Isolated qKO vacuoles show strongly impaired Ca^{2+} accumulation. Fura-2 fluorescence ratio recordings performed on (A) Col-0 vacuoles and (B) qKO Vacuoles, in response to bath application of 10 μ M or 30 μ M Ca^{2+} , as indicated (horizonal bars). Vacuoles were loaded with 100 μ M fura-2 through the patch pipette and kept at a membrane voltage of ~40 mV. Vacuolar fluorescence ratio values were converted into [Ca²⁺] units. (C) Summary plot showing the vacuolar [Ca²⁺] changes (Δ [Ca²⁺] ν ac) evoked by cytosolic Ca²⁺ application at 10 μ M (n=7 vacuoles for both Col-0 and qKO) or 30 μ M (n=14 Col-0 and 18 qKO). Data represent mean \pm sem. Wilcoxon Rank test: **P= 0.0034 for 10 μ M Ca²⁺ and **P=6×10⁻⁶ for 30 μ M Ca²⁺.



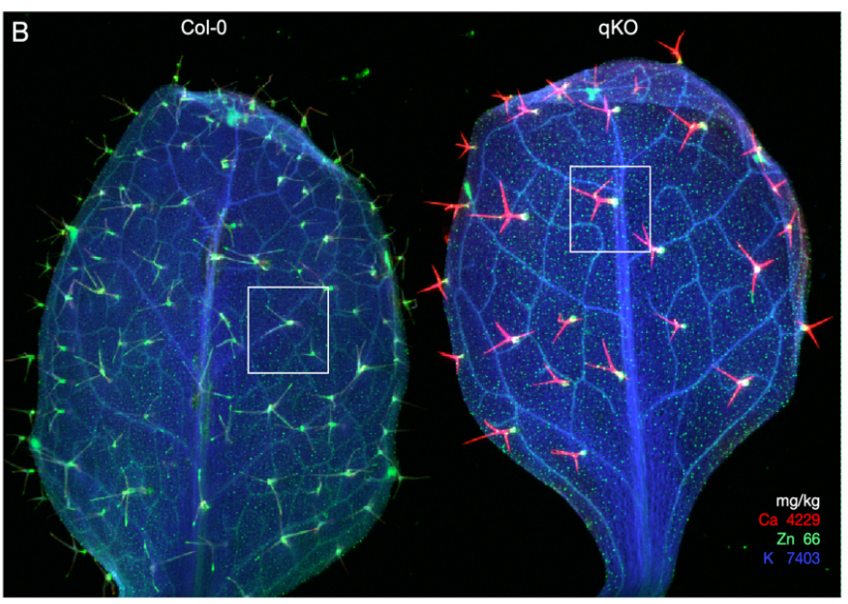
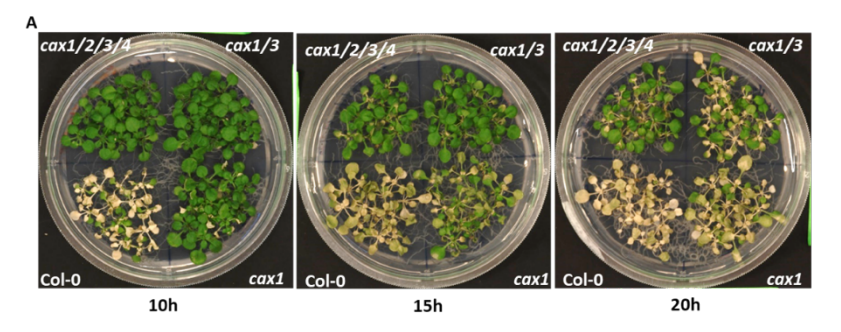
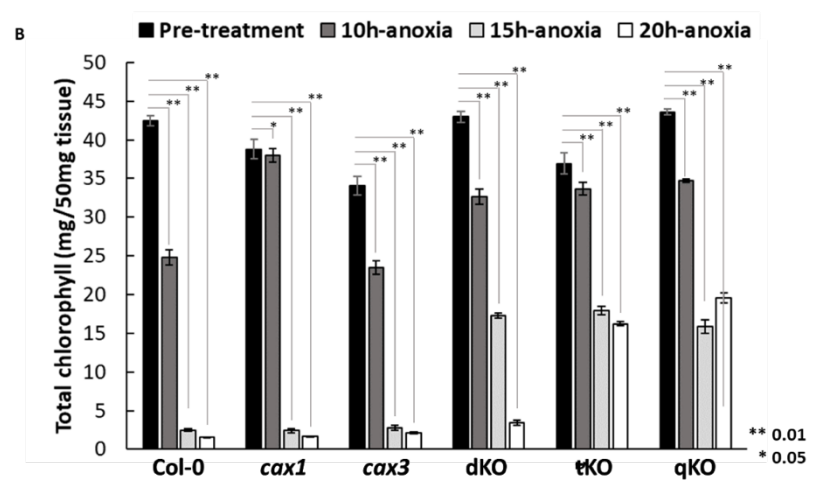


Figure 3. Bulk metal concentration and distribution in Col-0 and qKO leaves under normoxic growth conditions. A: Bulk Ca, Mg, K, Mn, Cu and Zn concentration of shoots (14 d) expressed as mg/kg, showing results of ANOVA statistical analysis, where letters denote results of Tukey's means separation. B: Tricolor SXRF elemental image of Ca (red), Zn (green) and K (blue) in 14 d old leaves of WT and QKO. Maximum values are shown as mg/kg. C & D: Zoomed in images of trichomes (white boxes), showing greater Ca in qKO. E: User-defined region of interest analysis of trichomes (N=5, expressed as ion chamber normalized fluorescence counts, averaged to the pixel area) showing results of ANOVA statistical analysis for Ca, Mn and Cl.





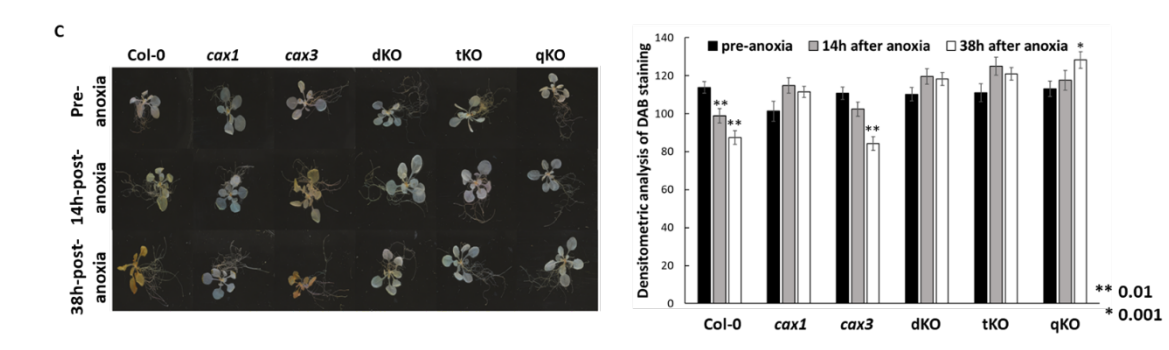


Figure 7. Anoxia response of CAX mutants. (A) Increased anoxia tolerance of dKO and qKO in comparison with cax1 mutant. cax1 plants lost their tolerance to anoxia after 15h of treatment, while qKO plants maintained their tolerance even after 20h of treatment. 21-day old plants (9 rosette leaf stage) were placed in a GasPack Anaerobic system and were taken out after 10, 15 and 20h of treatment. These plants were then returned to normoxic conditions and photographed after five days. Photographs represent more than 3 biological replicates. (B) Confirming the level of anoxia tolerance in cax1, dKO, tKO and qKO by chlorophyll estimation. tKO and qKO plants showed significantly lower chlorophyll loss than dKO after 20h of anoxia treatment. However, chlorophyll oss was comparable among these genotypes (dKO, tKO and tKO) after 15h of treatment. cax1 showed complete loss of chlorophyll after 15h of treatment. There was no significant difference in the levels of chlorophyll loss between tKO and qKO at any time points analyzed. Experiments were performed as mentioned in A. Data indicated is a representative of 3 biological replicates and asterisk indicate significant difference from the pre-treatment conditions as calculated by ANOVA asterisks (*, $P \le 0.05$ and **, $P \le 0.01$). Error bars represent standard error from the mean value. (C) Decreased H₂O₂ accumulation in the CAX mutants as indicated by 3,3'-diaminobenzidine (DAB) staining. A dark brown precipitate in Col-0 and cax3 indicate the presence of H₂O₂. Whole rosettes from 3-weeks old plants were exposed to anoxic conditions for 10h. Rosettes were sampled 14 and 38h after the plants were brought back to normoxic growth conditions. Unstressed plants (Pre-anoxia) were used as the control. Data shown is a representative of more than three independent experiments. (D) Quantification of DAB staining by software ImageJ. Nine leaves from three different plants were used for quantification. Asterisks indicate significant difference compared to pre-anoxia condition

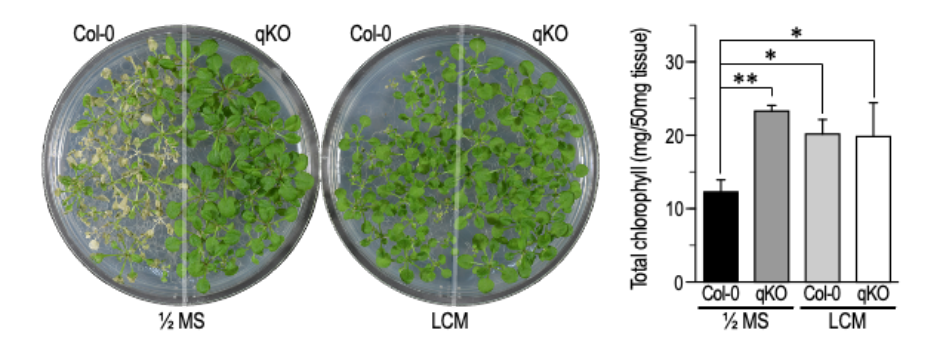
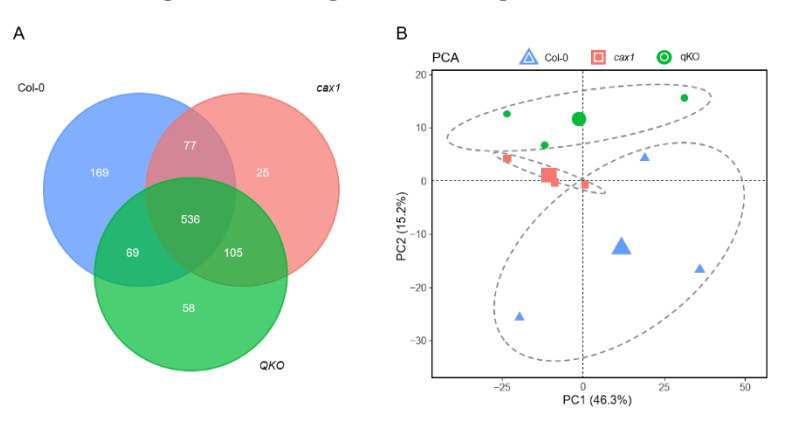


Figure 8. Anoxia response of Col-0 grown in low-calcium-containing media. (A) Increased anoxia tolerance of Col-0 grown in low-calcium containing media (LCM) compared to Col-0 grown in ½ MS. 21-day old plants (9 rosette leaf stage) were placed in a GasPack Anaerobic system and were taken out after 8h of treatment. These plants were then returned to normoxic conditions and photographed after four days. Photographs represent more than three biological replicates. (B) Confirming the anoxia tolerance by chlorophyll estimation. Col-0 in LCM and qKO plants grown in both media conditions showed significantly lower chlorophyll loss than Col-0 growth in ½ MS 20h post anoxia. Experiments were performed as mentioned in A. Data is representative of 3 replicates.



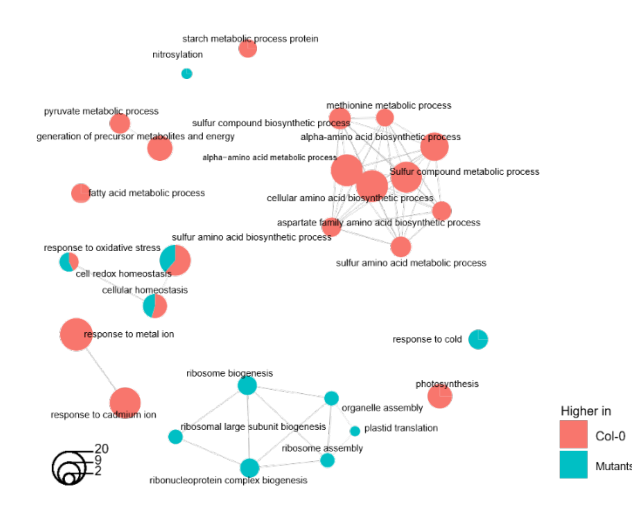
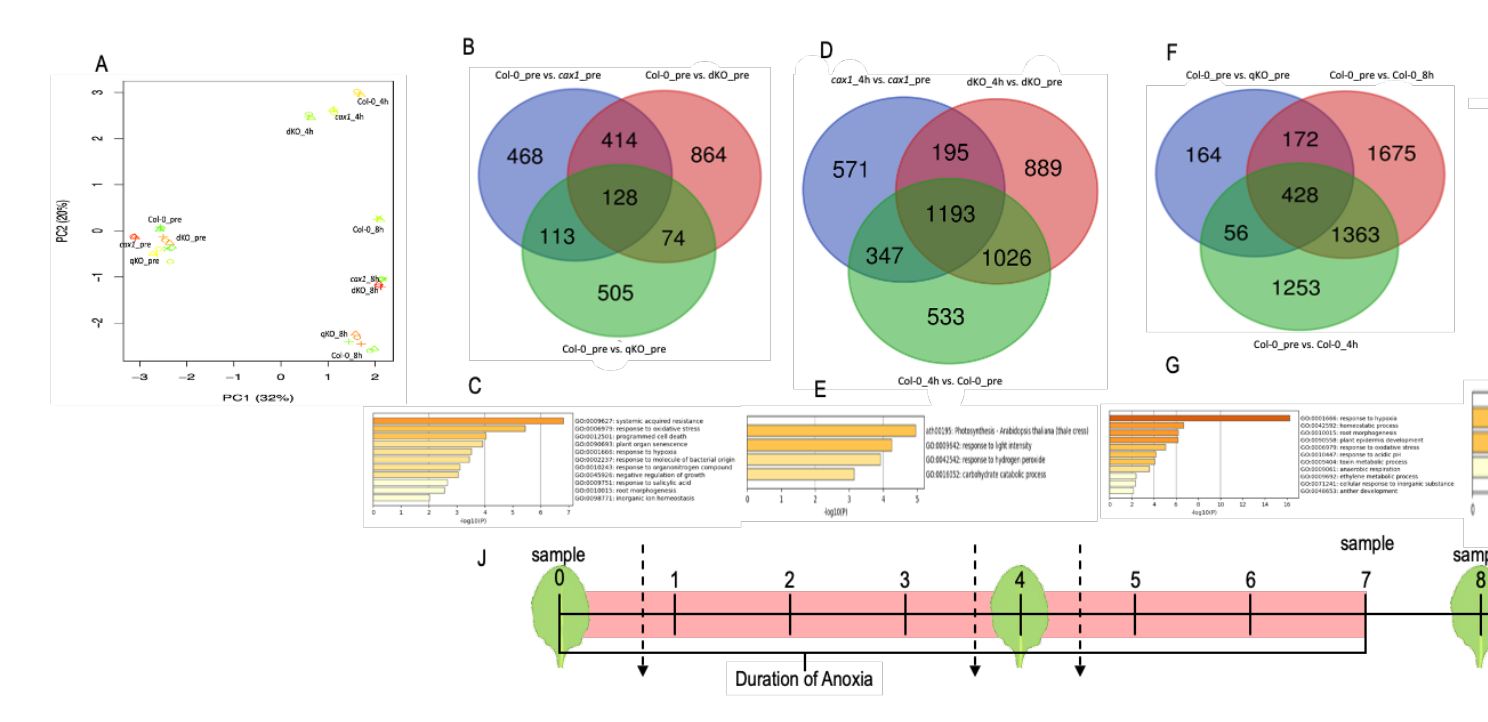


Figure 4. Proteomic analysis of Col-0, cax1, qko under normoxia condition. (A) Venn diagram showing the overlap between proteins identified in three lines. (B) Principle component analysis (PCA) of the proteome of Col-0, cax1, qko under normoxia condition. Sample scores for the first and second principal components were plotted, the explained percentage of variance of PC1 and PC2 are indicated along the x and y axes. Clusters corresponding to the groups are represented by 95% confidence ellipses and include data from three biological replicates. The enlarged dots represent the means of the groups. (C) Enrichment network depicting the significantly enriched GO biological process terms (hypergeometric test with Bonferroni correction, P < 0.05) for proteins with higher (blue) or lower (red) abundance in both mutants. Each GO term is represented by a circle, and different groups are shown as different colors. The size of the GO term circle reflects the number of genes/proteins enriched in the corresponding item.

С



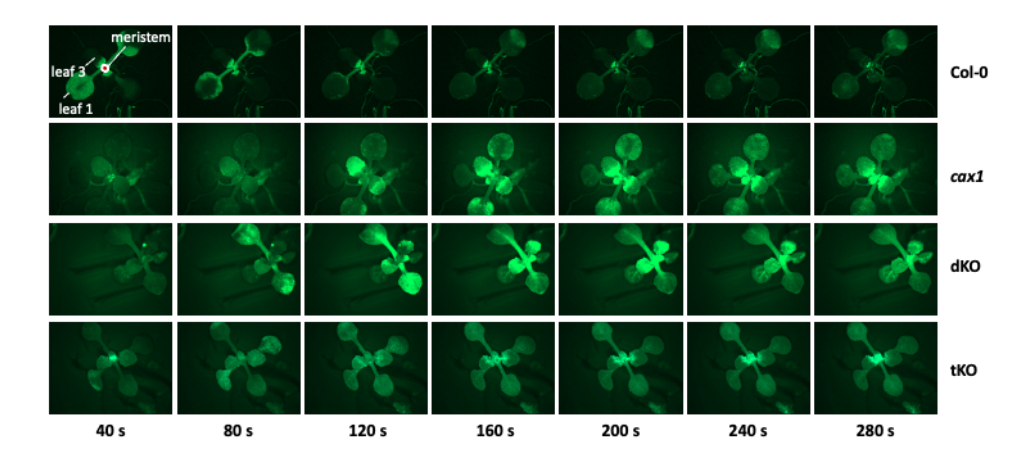
- Principal component analysis plot (PCA) representation of Col-0, cax1, cax1/3 and cax1/2/3/4 transcriptomes before, during and after anoxic treatment. Upregulated genes in cax1, dKO and qKO compared during normoxia condition. A. B.
- GO biological pathway analyses are for the 128 common upregulated genes in all the three mutant lines.
- Upregulated genes in Col-0, cax1 and dKO during anoxia.
- GO biological pathway analyses are for the 195 common upregulated genes in cax1 and dKO that are not found in Col-0. Upregulated genes in qKO during normoxia and Col-0 during and post-anoxia.
- GO biological pathway analyses are for the 428 common upregulated genes in qKO during normoxia and Col-0 during and post-anoxia.

- Upregulated genes in dKO and qKO compared to Col-Opost-anoxia.

 GO biological pathway analyses are for the 42 common upregulated genes in dKO and qKO.

 Scheme and timing of leaf tissue harvesting for RNA-seq analysis. Plants belonging to 9 rosette leaf stage were taken for RNA-seq analysis before anoxia (pre-conditions), after 4 hours of anoxia (anoxia) and 1 hour after a 7-hour anoxia treat

Α



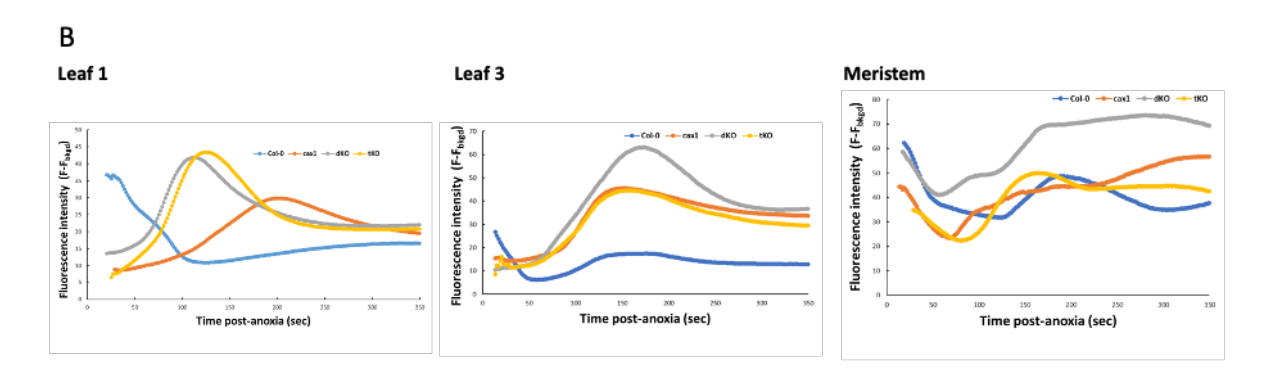


Figure 6. Calcium changes in Col-0, cax1, dKO and tKO during exposure to oxygen after anoxia stress. Col-0 , cax1, dKO and tKO stably expressing the genetically encoded Ca²+ indicator, GCaMP3 , were grown on 1/2MS with 0.5% sucrose for 12 days and were treated with anoxia stress for 4h. Intensity of fluorescence of GCaMP3 was recorded using a fluorescence microscope immediately after the plants were re-exposed to oxygen. (A) Representative images of plants expressing the GCaMP3 Ca²+ biosensor at different time points as 40, 80, 120, 160, 200, 240 and 280 seconds after exposing them to normoxic conditions. (B) Quantification of fluorescence of the selected genotypes during reoxygenation after anoxia stress. Region of interest is as outlined as in figure 1A. Representative of ≥3 independent plants/leaves.

Figure Legends

Figure 1. Growth characteristics of CAXs mutants. (A) Reduced growth of CAX mutants in media containing 25mM CaCl₂. Seeds were germinated and grown in half-MS medium for 15 days before they were transferred to medium containing calcium (lower panel). Photographs were taken 5 days after transferring to the supplemented medium. Control plants grown on half-MS medium for 20 days is given in the upper panel. (B) Reduced growth of CAX mutants in hydroponic basal nutrient solution (BNS) containing 1mM calcium. (C) Altered growth of dKO, tKO and qKO in soil. dKO, tKO and qKOs were much smaller than Col-0 and *cax1* single mutant. All these plants were grown on half-MS media for 10 days before transferring to soil.

 Figure 2. Isolated qKO vacuoles show strongly impaired Ca²⁺ accumulation. Fura-2 fluorescence ratio recordings performed on (A) Col-0 vacuoles and (B) qKO Vacuoles, in response to bath application of 10 μM or 30 μM Ca²⁺, as indicated (horizonal bars). Vacuoles were loaded with 100 μM fura-2 through the patch pipette and kept at a membrane voltage of ~40 mV. Vacuolar fluorescence ratio values were converted into [Ca²⁺] units. (C) Summary plot showing the vacuolar [Ca²⁺] changes (Δ [Ca²⁺]_{vac}) evoked by cytosolic Ca²⁺ application at 10 μM (n=7 vacuoles for both Col-0 and qKO) or 30 μM (n=14 Col-0 and 18 qKO). Data represent mean \pm sem. Wilcoxon Rank test: **P= 0.0034 for 10 μM Ca²⁺ and **P=6×10⁻⁶ for 30 μM Ca²⁺.

Figure 3. Bulk metal concentration and distribution in Col-0 and qKO leaves under normoxic growth conditions. (A) Bulk Ca, Mg, K, Mn, Cu and Zn concentration of shoots (14d) expressed as mg/kg, showing results of ANOVA statistical analysis, where letters denote results of Tukey's means separation. (B) Tricolor SXRF elemental image of Ca (red), Zn (green), and K (blue) in 14d old leaves of Col-0 and qKO. Maximum values are shown as mg/kg. (C,D) Zoomed in images of trichomes (white boxes), showing greater Ca in qKO. (E) User-defined region of interest analysis of trichomes (n=5, expressed as ion chamber normalized fluorescence counts, averaged to the pixel area) showing results of ANOVA statistical analysis for Ca, Mn and CL.

Figure 4. Proteomic analysis of Col-0, cax1 and qko under normoxia condition. (A) Venn diagram showing the overlap between proteins identified in three lines. (B) Principal component analysis (PCA) of the proteome of Col-0, cax1, qko under normoxia condition. Sample scores for the first and second principal components were plotted, the explained percentage of variance of PC1 and PC2 are indicated along the x and y axes. Clusters corresponding to the groups are represented by 95% confidence ellipses and include data from three biological replicates. The enlarged dots represent the means of the groups. (C) Enrichment network depicting the significantly enriched GO biological process terms (hypergeometric test with Bonferroni correction, P < 0.05) for proteins with higher (blue) or lower (red) abundance in both mutants. Each GO term is represented by a circle, and different groups are shown as different colours. The size of the GO term circle reflects the number of genes/proteins enriched in the corresponding item.

Figure 5. CAXs mutants transcriptome-wide responses to anoxia.

- A. Principal component analysis plot (PCA) representation of Col-0, *cax1*, *cax1/3* and *cax1/2/3/4* transcriptomes before, during and after anoxic treatment.
- B. Upregulated genes in cax1, dKO and qKO compared during normoxia condition.
- C. GO biological pathway analyses are for the 128 common upregulated genes in all the three mutant lines.

D. Upregulated genes in Col-0, *cax1* and dKO during anoxia.

- E. GO biological pathway analyses are for the 195 common upregulated genes in *cax1* and dKO that are not found in Col-0.
- F. Upregulated genes in qKO during normoxia and Col-0 during and post-anoxia.
- G. GO biological pathway analyses are for the 428 common upregulated genes in qKO during normoxia and Col-0 during and post-anoxia.
- H. Upregulated genes in dKO and qKO compared to Col-0post-anoxia.
- I. GO biological pathway analyses are for the 42 common upregulated genes in dKO and gKO.
- J. Scheme and timing of leaf tissue harvesting for RNA-seq analysis. Plants belonging to 9 rosette leaf stage were taken for RNA-seq analysis before anoxia (pre-conditions), after 4 hours of anoxia (anoxia) and 1 hour after a 7-hour anoxia treatment (post-anoxia).

Figure 6. Calcium changes in Col-0, *cax1*, dKO and tKO during exposure to oxygen after anoxia stress. Col-0, *cax1*, dKO and tKO stably expressing the genetically encoded Ca²⁺ indicator, GCaMP3, were grown on 1/2MS with 0.5% sucrose for 12 days and were treated with anoxia stress for 4h. Intensity of fluorescence of GCaMP3 was recorded using a fluorescence microscope immediately after the plants were re-exposed to oxygen. (A) Representative images of plants expressing the GCaMP3 Ca²⁺ biosensor at different time points as 40, 80, 120, 160, 200, 240 and 280 seconds after exposing them to normoxic conditions. (B) Quantification of fluorescence of the selected genotypes during reoxygenation after anoxia stress. Region of interest is as outlined as in figure 1A. Representative of ≥3 independent plants/leaves.

Figure 7. Anoxia response of CAX mutants. (A) Increased anoxia tolerance of dKO and qKO in comparison with cax1 mutant. cax1 plants lost their tolerance to anoxia after 15h of treatment, while gKO plants maintained their tolerance even after 20h of treatment. 21-day old plants (9 rosette leaf stage) were placed in a GasPack Anaerobic system and were taken out after 10, 15 and 20h of treatment. These plants were then returned to normoxic conditions and photographed after five days. Photographs represent more than 3 biological replicates. (B) Confirming the level of anoxia tolerance in cax1, dKO, tKO and gKO by chlorophyll estimation. tKO and qKO plants showed significantly lower chlorophyll loss than dKO after 20h of anoxia treatment. However, chlorophyll loss was comparable among these genotypes (dKO, tKO and tKO) after 15h of treatment. cax1 showed complete loss of chlorophyll after 15h of treatment. There was no significant difference in the levels of chlorophyll loss between tKO and qKO at any time points analyzed. Experiments were performed as mentioned in A. Data indicated is a representative of 3 biological replicates and asterisk indicate significant difference from the pretreatment conditions as calculated by ANOVA asterisks (*, P ≤ 0.05 and **, P ≤ 0.01). Error bars represent standard error from the mean value. (C) Decreased H₂O₂ accumulation in the CAX mutants as indicated by3,3'-diaminobenzidine (DAB) staining. A dark brown precipitate in Col-0 and cax3 indicate the presence of H₂O₂. Whole rosettes from 3-weeks old plants were exposed to anoxic conditions for 10h. Rosettes were sampled 14 and 38h after the plants were brought back to normoxic growth conditions. Unstressed plants (Pre-anoxia) were used as the control. Data shown is a representative of more than three independent experiments. (D) Quantification of DAB staining by software ImageJ. Nine leaves from three different plants were used for quantification. Asterisks indicate significant difference compared to pre-anoxia condition as calculated using Student's T-test in Excel (*, $P \le 0.01$ and **, $P \le 0.001$).

- Figure 8. Anoxia response of Col-0 grown in low-calcium-containing media. (A) Increased anoxia tolerance of Col-0 grown in low-calcium containing media (LCM) compared to Col-0 grown
- 894 in ½ MS. 21-day old plants (9 rosette leaf stage) were placed in a GasPack Anaerobic system
- and were taken out after 8h of treatment. These plants were then returned to normoxic conditions and photographed after four days. Photographs represent more than three biological replicates.
- 897 (B) Confirming the anoxia tolerance by chlorophyll estimation. Col-0 in LCM and gKO plants
- grown in both media conditions showed significantly lower chlorophyll loss than Col-0 growth in
- 899 ½ MS 20h post anoxia. Experiments were performed as mentioned in A. Data is representative

900 of 3 replicates.

901 902 REFERENCES

702 NEI ENENOLE

- 903 1. Arnon DI. 1949. Copper Enzymes in Isolated Chloroplasts. Polyphenoloxidase in Beta Vulgaris. *Plant Physiol* 24:1-15
- Baliardini C, Corso M, Verbruggen N. 2016. Transcriptomic analysis supports the role of CATION EXCHANGER 1 in cellular homeostasis and oxidative stress limitation during cadmium stress. *Plant Signaling & Behavior* EPub Ahead of Print - ACCEPTED Manuscript:0
- Baliardini C, Meyer CL, Salis P, Saumitou-Laprade P, Verbruggen N. 2015. CATION
 EXCHANGER1 Cosegregates with Cadmium Tolerance in the Metal Hyperaccumulator
 Arabidopsis halleri and Plays a Role in Limiting Oxidative Stress in Arabidopsis Spp.
 Plant Physiol 169:549-59
- 913 4. Barkla BJ, Vera-Estrella R, Hernandez-Coronado M, Pantoja O. 2009. Quantitative 914 proteomics of the tonoplast reveals a role for glycolytic enzymes in salt tolerance. *Plant* 915 *Cell* 21:4044-58
- 916 5. Berridge MJ, Lipp P, Bootman MD. 2000. The versatility and universality of calcium signalling. *Nature Reviews-Molecular Cell Biology* 1:11-21
- 918 6. Bradshaw HD, Jr. 2005. Mutations in *CAX1* produce phenotypes characteristic of plants tolerant to serpentine soils. *New Phytologist* 167:81-8
- 920 7. Broadhurst CL, Chaney RL, Angle JS, Maugel TK, Erbe EF, Murphy CA. 2004.
- 921 Simultaneous Hyperaccumulation of Nickel, Manganese, and Calcium in Alyssum Leaf 922 Trichomes. *Environmental Science & Technology* 38:5797-802
- 923 8. Cai X, Lytton J. 2004. The Cation/Ca²⁺ exchanger superfamily: Phylogenetic analysis and structural implications. *Molecular Biology and Evolution* 21:1692-703
- 925 9. Carpaneto A, Boccaccio A, Lagostena L, Di Zanni E, Scholz-Starke J. 2017. The 926 signaling lipid phosphatidylinositol-3,5-bisphosphate targets plant CLC-a anion/H(+) 927 exchange activity. *EMBO reports* 18:1100-7
- 928 10. Catalá R, Santos E, Alonso JM, Ecker JR, Martinez-Zapater JM, Salinas J. 2003.
- Mutations in the Ca²⁺/H⁺ transporter CAX1 increase *CBF/DREB1* expression and the cold-acclimation response in Arabidopsis. *Plant Cell* 15:2940-51
- 931 11. Cheng N-H, Pittman JK, Barkla BJ, Shigaki T, Hirschi KD. 2003. The Arabidopsis cax1
 932 mutant exhibits impaired ion homeostasis, development, and hormonal responses and
- reveals interplay among vacuolar transporters. *Plant Cell* 15:347-64
- 934 12. Cheng N-H, Pittman JK, Shigaki T, Lachmansingh J, LeClere S, et al. 2005. Functional
- association of Arabidopsis CAX1 and CAX3 Is required for normal growth and ion homeostasis. *Plant Physiology* 138:2048-60

- 937 13. Cho D, Villiers F, Kroniewicz L, Lee S, Seo YJ, et al. 2012. Vacuolar CAX1 and CAX3
 938 influence auxin transport in guard cells via regulation of apoplastic pH. *Plant Physiol*939 160:1293-302
- 940 14. Clemens S. 2006. Toxic metal accumulation, responses to exposure and mechanisms of tolerance in plants. *Biochimie* 88:1707-19
- Colmenero-Flores JM, Franco-Navarro JD, Cubero-Font P, Peinado-Torrubia P, Rosales
 MA. 2019. Chloride as a Beneficial Macronutrient in Higher Plants: New Roles and
 Regulation. *International journal of molecular sciences* 20
- 945 16. Conn SJ, Gilliham M, Athman A, Schreiber AW, Baumann U, et al. 2011. Cell-specific vacuolar calcium storage mediated by *CAX1* regulates apoplastic calcium concentration, gas exchange, and plant productivity in *Arabidopsis*. *Plant Cell* 23:240-57
- 948 17. Costa A, Navazio L, Szabo I. 2018. The contribution of organelles to plant intracellular Calcium signalling. *J Exp Bot*
- 950 18. Demidchik V, Shabala S, Isayenkov S, Cuin TA, Pottosin I. 2018. Calcium transport across plant membranes: mechanisms and functions. *New Phytol* 220:49-69
- 952 19. Dobin A, Davis CA, Schlesinger F, Drenkow J, Zaleski C, et al. 2013. STAR: ultrafast
 953 universal RNA-seq aligner. *Bioinformatics* 29:15-21
- 20. Eisenach C, Baetz U, Martinoia E. 2014. Vacuolar proton pumping: More than the sum
 of its parts? *Trends in Plant Science* 19:344-6
- 956 21. Fones HN, Preston GM, Smith JAC. 2019. Variation in defence strategies in the metal hyperaccumulator plant Noccaea caerulescens is indicative of synergies and trade-offs between forms of defence. *R Soc Open Sci* 6:172418
- 959 22. Gradogna A, Scholz-Starke J, Gutla PV, Carpaneto A. 2009. Fluorescence combined with excised patch: measuring calcium currents in plant cation channels. *Plant J* 58:175-82
- Gradogna A, Scholz-Starke J, Pardo JM, Carpaneto A. 2021. Beyond the patch-clamp
 resolution: functional activity of nonelectrogenic vacuolar NHX proton/potassium
 antiporters and inhibition by phosphoinositides. *New Phytol* 229:3026-36
- 964 24. Grynkiewicz G, Poenie M, Tsien RY. 1985. A new generation of Ca2+ indicators with greatly improved fluorescence properties. *J Biol Chem* 260:3440-50
- Hindt MN, Akmakjian GZ, Pivarski KL, Punshon T, Baxter I, et al. 2017. BRUTUS and its paralogs, BTS LIKE1 and BTS LIKE2, encode important negative regulators of the iron deficiency response in Arabidopsis thaliana. *Metallomics* 9:876-90
- 969 26. Hirschi KD. 2004. The calcium conundrum: Both versatile nutrient and specific signal. 970 Plant Physiology 136:2438-42
- 971 27. Hirschi KD, Zhen R-G, Cunningham KW, Rea PA, Fink GR. 1996. CAX1, an H⁺/Ca²⁺
 972 antiporter from *Arabidopsis*. *Proceedings of the National Academy of Sciences*, *USA* 973 (*Plant Biology*) 93:8782-6
- 974 28. Hocking B, Conn SJ, Manohar M, Xu B, Athman A, et al. 2017. Heterodimerization of Arabidopsis calcium/proton exchangers contributes to regulation of guard cell dynamics and plant defense responses. *J Exp Bot* 68:4171-83
- 977 29. Hogan PG, Rao A. 2015. Store-operated calcium entry: Mechanisms and modulation.
 978 *Biochem Biophys Res Commun* 460:40-9
- Hu S, Peng L, Kwak Y-T, Tekippe EM, Pasare C, et al. 2015. The DNA sensor AIM2
 maintains intestinal homeostasis via regulation of epithelial antimicrobial host defense.
 Cell reports 13:1922-36

- 982 31. Liang Y, Urano D, Liao KL, Hedrick TL, Gao Y, Jones AM. 2017. A nondestructive 983 method to estimate the chlorophyll content of Arabidopsis seedlings. *Plant Methods* 984 13:26
- Signature
 Liu T-Y, Aung K, Tseng C-Y, Chang T-Y, Chen Y-S, Chiou T-J. 2011. Vacuolar Ca²⁺/H⁺ transport activity is required for systemic phosphate homeostasis involving shoot-to-root signaling in Arabidopsis. *Plant Physiology* 156:1176-89
- 988 33. Manohar M, Shigaki T, Hirschi KD. 2011. Plant cation/H⁺ exchangers (CAXs):
 989 Biological functions and genetic manipulations. *Plant Biology (Stuttg), Germany* 13:561990 9
- 991 34. Manohar M, Shigaki T, Mei H, Park S, Marshall J, et al. 2011. Characterization of 992 *Arabidopsis* Ca²⁺/H⁺ exchanger CAX3. *Biochemistry* 50:6189-95
- 993 35. Marty F. 1999. Plant Vacuoles. *Plant Cell* 11:587-600
- 994 36. Modareszadeh M, Bahmani R, Kim D, Hwang S. 2021. CAX3 (cation/proton exchanger) 995 mediates a Cd tolerance by decreasing ROS through Ca elevation in Arabidopsis. *Plant* 996 *Mol Biol* 105:115-32
- 997 37. Noctor G, Lelarge-Trouverie C, Mhamdi A. 2015. The metabolomics of oxidative stress. *Phytochemistry* 112:33-53
- 999 38. Paradiso A, Caretto S, Leone A, Bove A, Nisi R, De Gara L. 2016. ROS Production and Scavenging under Anoxia and Re-Oxygenation in Arabidopsis Cells: A Balance between Redox Signaling and Impairment. *Frontiers in plant science* 7:1803
- 1002 39. Pertea M, Pertea GM, Antonescu CM, Chang TC, Mendell JT, Salzberg SL. 2015.
 1003 StringTie enables improved reconstruction of a transcriptome from RNA-seq reads. *Nat Biotechnol* 33:290-5
- 1005 40. Pittman JK, Hirschi KD. 2016. CAX-ing a wide net: Cation/H transporters in metal remediation and abiotic stress signalling. *Plant Biology (Stuttg)* 18:741-9
- 1007 41. Pittman JK, Hirschi KD. 2016. Phylogenetic analysis and protein structure modelling identifies distinct Ca(2+)/Cation antiporters and conservation of gene family structure within Arabidopsis and rice species. *Rice (N Y)* 9:1-6
- 1010 42. Pittman JK, Shigaki T, Hirschi KD. 2005. Evidence of differential pH regulation of the Arabidopsis vacuolar Ca2+/H+ antiporters CAX1 and CAX2. FEBS Letters 579:2648-56
- Punshon T, Hirschi K, Yang J, Lanzirotti A, Lai B, Guerinot ML. 2012. The role of
 CAX1 and CAX3 in elemental distribution and abundance in Arabidopsis seed. *Plant Physiology* 158:352-62
- 1015 44. Ricachenevsky FK, Punshon T, Salt DE, Fett JP, Guerinot ML. 2021. Arabidopsis thaliana zinc accumulation in leaf trichomes is correlated with zinc concentration in leaves. *Sci Rep* 11:5278
- Sanders D, Pelloux J, Brownlee C, Harper JF. 2002. Calcium at the Crossroads of Signaling. *Plant Cell* 14:S401-17
- 1020 46. Schachtman DP, Shin R. 2007. Nutrient sensing and signaling: NPKS. *Annual Reviews* 1021 of Plant Biology 58:47-69
- 1022 47. Schonknecht G. 2013. Calcium Signals from the Vacuole. *Plants (Basel)* 2:589-614
- 1023 48. Strazzer P, Spelt CE, Li S, Bliek M, Federici CT, et al. 2019. Hyperacidification of Citrus fruits by a vacuolar proton-pumping P-ATPase complex. *Nat Commun* 10:744
- 1025 49. Sze H, Chanroj S. 2018. Plant Endomembrane Dynamics: Studies of K(+)/H(+)
- 1026 Antiporters Provide Insights on the Effects of pH and Ion Homeostasis. *Plant Physiol* 1027 177:875-95

- 1028 50. Sze H, Li X, Palmgren MG. 1999. Energization of plant cell membranes by H⁺-pumping ATPases: Regulation and biosynthesis. *Plant Cell* 11:677-90
- Sze H, Liang F, Hwang I, Curran AC, Harper JF. 2000. DIVERSITY AND
 REGULATION OF PLANT Ca2+ PUMPS: Insights from Expression in Yeast. *Annual Review of Plant Physiology and Plant Molecular Biology* 51:433-62
- Whitt L, Ricachenevsky FK, Ziegler GZ, Clemens S, Walker E, et al. 2020. A curated list of genes that affect the plant ionome. *Plant Direct* 4:e00272
- 1035 53. Yang J, Mathew IE, Rhein H, Barker R, Guo Q, et al. 2022. The vacuolar H+/Ca 1036 transporter CAX1 participates in submergence and anoxia stress responses. *Plant Physiol* 1037 190:2617-36

 $\begin{array}{c} 1039 \\ 1040 \end{array}$